Title: Human intestinal enteroids with inducible neurogenin-3 expression as a novel model of gut hormone secretion

Short Title: *NGN3* enteroids as an enteroendocrine cell model

Authors: Alexandra L. Chang-Graham[1]*, Heather A. Danhof[1]*, Melinda A. Engevik[2,3]*, Catherine Tomaro-Duchesneau[1*], Umesh C. Karandikar[1], Mary K. Estes[1,4], James Versalovic[2,3], Robert A. Britton[1#], Joseph M. Hyser[1#]

*Authors contributed equally to this work

[1]Department of Molecular Virology and Microbiology, Baylor College of Medicine
[2]Department of Pathology and Immunology, Baylor College of Medicine
[3]Department of Pathology, Texas Children's Hospital
[4]Department of Medicine, Gastroenterology and Hepatology, Baylor College of Medicine

 # Joint Corresponding Authors:
Joseph M. Hyser, Ph.D.
Assistant Professor
Alkek Center for Metagenomics and Microbiome Research
Department of Molecular Virology and Microbiology
Baylor College of Medicine
One Baylor Plaza, MS: BCM385
Tel: 713-798-4514
Fax: 713-798-3586
Joseph.hyser@bcm.edu

Robert A. Britton, Ph.D.
Professor
Alkek Center for Metagenomics and Microbiome Research
Department of Molecular Virology and Microbiology
Baylor College of Medicine
One Baylor Plaza, MS: BCM385
Tel: 713-798-6189
Fax: 713-798-3586
Robert.Britton@bcm.edu

Grant Support:
Funding support includes: NIH F30DK112563 (A.C.G), Fonds de recherche santé Québec (C.T.D.), NIH U01CA170930 (J.V.), NIH R01DK103759 (R.A.B), NIH U19 AI116497, R01 AI080656 (M.K.E.), and NIH R03DK110270 and Baylor College of Medicine (BCM) Seed Funding (J.M.H.). This project was also supported in part by the NIH PHS grant P30 DK056338 for the Texas Medical Center Digestive Diseases Center. Additional funding support for the BCM Integrated Microscopy Core includes the NIH (DK56338, CA125123), CPRIT (RP150578, RP170719), the Dan L. Duncan

Comprehensive Cancer Center, and the John S. Dunn Gulf Coast Consortium for Chemical Genomics.

Disclosures:
No conflicts of interest exist.

Author Contributions:
Concept and design (ACG, HAD, MAE, CTD, UCK, MKE, RAB, JMH); intellectual contribution (ACG, HAD, MAE, CTD, UCK, MKE, JV, RAB, JMH); data acquisition (ACG, HAD, MAE, CTD, UCK); data analysis, statistical analysis, and interpretation (ACG, HAD, MAE, CTD, UCK); drafting and editing manuscript (ACG, HAD, MAE, JMH); obtained funding (MKE, JV, RAB, JMH)

Abbreviations: neurogenin-3 (NGN3), tetracycline (tet), doxycycline (dox), gastrointestinal (GI), human intestinal enteroids (HIEs), human intestinal organoids (HIOs), short chain fatty acids (SCFAs), chromogranin A (ChgA), pancreatic polypeptide (PP), glucose-dependent insulinotropic peptide (GIP), glucagon-like peptide-1 (GLP-1), peptide YY (PYY), monocyte chemoattractant protein-1 (MCP-1), tryptophan hydroxylase (Tph1), villin (VIL1), sucrase isomaltase (SI), rotavirus (RV), hour (hr), hours post infection (hpi), reverse transcriptase – quantitative polymerase chain reaction (RT-qPCR), immunofluorescence (IF), hematoxylin and eosin (H&E), two-dimensional (2D), three-dimensional (3D), complete medium without growth factors (CMGF-), complete media with growth factors (CMGF+), high Wnt complete media with growth factors (hW-CMGF+)

Word Count: 4368

72 **Synopsis:** Enteroendocrine cells have low abundance but exert widespread effects on
73 gastrointestinal physiology. We engineered human intestinal enteroids with inducible
74 expression of neurogenin-3, resulting in increased enteroendocrine cells and facilitating
75 investigations of host responses to the dynamic intestinal environment.

76

Abstract

Background: Enteroendocrine cells (EECs) are specialized epithelial cells that produce molecules vital for intestinal homeostasis, but due to their limited numbers, in-depth functional studies have remained challenging. Human intestinal enteroids (HIEs) that are derived from intestinal crypt stem cells are a biologically relevant *in vitro* model of the intestinal epithelium. HIEs contain all intestinal epithelial cell types; however, like the intestine, HIEs spontaneously produce few EECs, which limits their study.

Methods: To increase the number of EECs in HIEs, we used lentivirus transduction to stably engineer jejunal HIEs with doxycycline-inducible expression of neurogenin-3 (*NGN3*), a transcription factor that drives EEC differentiation (tet*NGN3*-HIEs). We examined the impact of *NGN3* induction on EECs by quantifying the increase in the enterochromaffin cells and other EEC subtypes. We functionally assessed secretion of serotonin and EEC hormones in response to norepinephrine and rotavirus infection.

Results: Treating tet*NGN3*-HIEs with doxycycline induced a dose-dependent increase of chromogranin A (ChgA)-positive and serotonin-positive cells, demonstrating increased enterochromaffin cell differentiation. Despite increased ChgA-positive cells, other differentiated cell types of the epithelium remained largely unchanged by gene expression and immunostaining. RNA sequencing of doxycycline-induced tet*NGN3*-HIEs identified increased expression of key hormones and enzymes associated with several other EEC subtypes. Doxycycline-induced tet*NGN3*-HIEs secreted serotonin, monocyte chemoattractant protein-1, glucose-dependent insulinotropic peptide, peptide

YY, and ghrelin in response to norepinephrine and rotavirus infection, further supporting the presence of multiple EEC types.

Conclusions: We have combined HIEs and inducible-*NGN3* expression to establish a flexible *in vitro* model system for functional studies of EECs in enteroids and advance the molecular and physiological investigation of EECs.

Keywords**:** enteroendocrine cell; enteroid; serotonin

Introduction

The gastrointestinal (GI) epithelium is the largest sensory interface between host and environment and must both detect and communicate luminal contents to the host [1]. The GI lumen is a complex mixture of dietary nutrients and their breakdown products, microorganisms and their metabolites, as well as irritants, toxins, and drugs. Microorganisms in particular create a dynamic ecosystem in the GI lumen with both beneficial and detrimental effects. For example, the gut microbiome is important for degradation of complex carbohydrates and polysaccharides into short chain fatty acids (SCFAs) such as acetate, butyrate, and propionate that can be used as nutrients by the host or other microbes. SCFAs also modulate a variety of important physiological effects such as inflammation and gut motility [2]. By contrast, pathogenic microorganisms invade the epithelium or produce toxins that threaten the GI epithelial barrier and thus necessitate activation of host defenses. Therefore, integrating signals from luminal stimuli to the host for coordinated and appropriate physiological responses is complex, which has complicated efforts to study the molecular mechanisms governing these processes.

Microbiome-to-epithelium communication is multifaceted and includes receptors on various cell types, including enterocytes, goblet cells, Paneth cells and stem cells. Recent evidence shows that enteroendocrine cells are one of the most important mediators of communication between the GI lumen and host [3]. Enteroendocrine cells (EECs) are a rare cell lineage found throughout the length of the GI tract (<1% of GI epithelial cells), yet they have a significant impact on human physiology [4-6]. In response to host, microbial, and environmental stimuli, subtypes of EECs synthesize

and secrete hormones including gastrin (G cells), somatostatin (D cells), enteroglucagon/peptide YY (PYY) and glucagon-like peptide 1 (GLP-1) (L cells), neurotensin (N cells), pro-γ-melanocyte-stimulating hormone (MSH) cells, and serotonin (enterochromaffin cells) [7-9]. The broad array of enteroendocrine cell types reflects the diversity of critical physiological functions including the coordination of both local and systemic responses by the endocrine and nervous systems to the stimuli present in the lumen. Enterochromaffin cells are the most common EEC subtype, comprising ~40% of the EECs. These cells synthesize and secrete the neurotransmitter serotonin in response to various physiological stimuli, including microbial metabolites, irritants, toxins, and infection [10-12]. Given the importance of serotonin in mammalian physiology and greater abundance among EECs, many studies focus on enterochromaffin cells, but due in part to their rarity, how other EEC subtypes function in the context of the gut environment remains less well studied.

Studying the interaction of EECs and stimuli in the GI lumen has been challenging due to the limited numbers of these cells in the intestinal epithelium and the lack of appropriate non-cancer derived *in vitro* models. Generation of enteroids is a recent technology that has revolutionized the study of intestinal epithelial cells. They have been generated from several mammalian hosts, including mouse and human, and recapitulate the GI physiology of the donor species [13-16]. This complex epithelial culture system is derived from adult stem cells isolated from intestinal tissue or biopsy samples that can be maintained and expanded in culture as an *in vitro* model system [13-15, 17-21]. Thus, enteroids offer a promising new tool to study non-transformed, non-cancerous human EECs in an *in vitro* culture system [17].

155 Previous studies have established that neurogenin 3 (Ngn3) is a key transcription
156 factor for EEC differentiation [22-36]. Consistent with the role of Ngn3 in EEC fate,
157 overexpression of *NGN3* in multiple systems has been shown to increase EEC numbers
158 [37, 38]. *In vitro*, adenoviral-based *NGN3* overexpression in neonatal mouse jejunal
159 intestinal spheres induced a threefold increase in the number of chromogranin A
160 (ChgA)–positive EECs [39]. In human intestinal organoids (HIOs) derived from
161 pluripotent stem cells, overexpression of *NGN3* by an adenoviral vector or tetracycline-
162 inducible lentiviral vector also increased ChgA-positive EECs [29, 40]. In this study, we
163 generated a new model system using jejunal human intestinal enteroids (HIEs)
164 engineered to overexpress *NGN3* from a tetracycline-inducible promoter (tet*NGN3*) to
165 drive EEC differentiation. These tet*NGN3*-HIEs exhibit a doxycycline dose-dependent
166 increase in ChgA expression in both 3-dimensional culture and as 2-dimensional
167 monolayers, as well as upregulation of markers for multiple EEC subtypes, including
168 enterochromaffin cells, L cells and K cells. In response to microbial and host stimuli,
169 these induced EECs secreted serotonin, monocyte chemoattractant protein-1 (MCP-1),
170 glucose-dependent insulinotropic peptide (GIP), peptide YY (PYY), and ghrelin. Thus,
171 tet*NGN3*-HIEs are a new and physiologically relevant model system to study EEC-
172 based communication pathways in response to both microbial and host stimuli.
173

Results

Creation and propagation of inducible tetNGN3-HIEs

Since host-microbe interactions via EECs has a profound impact on host physiology, we sought to develop a new model for screening, identification, and testing of microbe-induced EEC responses. Due to the low abundance of EECs within intestinal tissue and human intestinal enteroids (HIEs), we aimed to increase EEC abundance through inducible overexpression of *NGN3* using lentivirus transduction to introduce a doxycycline-inducible NGN3 expression cassette into an HIE [72, 73]. In preparation for transduction, jejunal HIEs were grown high Wnt complete media with growth factors (hW-CMGF+) to enrich the stem cell population, which was evidenced by the majority of HIEs exhibiting a cystic morphology with multiple small buds (**Fig. 1A, left panel**). Growth in high Wnt media was important for increasing the success rate of the transduction. After lentivirus transduction, geneticin selection initially increased sloughing of dead cells from the HIEs, and full selection of transduced tet*NGN3*-HIEs occurred after ~5 weeks (**Fig. 1A, right panel**).

To confirm the ability of *NGN3* to drive EEC differentiation we used immunofluorescence (IF) staining for chromogranin A (ChgA) as a marker of endocrine cells, which are often used to assess increases in EEC numbers upon *NGN3* overexpression [29, 39, 40]. First, the number of ChgA-positive cells present in the tet*NGN3*-HIEs after induction with 1 µg/mL doxycycline was assessed (**Fig. 1B**). In paraffin-embedded slices of 3D tet*NGN3*-HIE cultures, we observed abundant ChgA-positive cells in both apical and basolateral areas of cells (**Fig 1B**). In contrast to the doxycycline-induced tet*NGN3*-HIEs, very few ChgA-positive cells were observed in the

absence of doxycycline (**Fig. 1C**, **left panel**). However, induction of tet*NGN3* increased the number of ChgA-positive cells in a doxycycline dose-dependent manner (**Fig. 1C**). A similar doxycycline dose-dependent increase in ChgA-positive cells was observed in two-dimensional (2D) flat monolayers (**Fig. 1D**). Of note, the ChgA-positive cells in both 3D and 2D formats exhibited the polygonal cell shape typically associated with enterochromaffin cells [41].

Using image analysis software, we quantified the abundance of ChgA-positive cells from the different doxycycline-induction conditions above. In the absence of doxycycline, both 3D and monolayer tet*NGN3*-HIEs exhibited few to no ChgA-positive cells. In contrast, addition of 0.1 µg/mL and 1 µg/mL doxycycline to 3D tet*NGN3*-HIEs resulted in a dose-dependent increase in the number of ChgA-positive cells ($p<0.0001$) (**Fig. 2A, left panel**). This pattern was also observed in 2D flat tet*NGN3*-HIEs monolayers, with doxycycline concentrations at or below 0.01 µg/mL exhibiting ~0.4% ChgA-positive cells, similar to the non-induced tet*NGN3*-HIEs (**Fig. 2A, right panel**). Treatment of tet*NGN3*-HIEs with 0.1 µg/mL doxycycline resulted in ~5% ChgA-positive cells, about a 12-fold increase, while addition of 1 µg/mL doxycycline resulted in ~40% ChgA-positive cells (**Fig. 2A right panel**). Thus, induction of tet*NGN3* correlated with an increase in ChgA-positive cells, supporting our premise that overexpression of *NGN3* would drive EEC differentiation in HIEs. The tet*NGN3*-HIEs have stably maintained the tet*NGN3* transgene and exhibited the doxycycline-induced increase in ChgA-positive cells (detected by IF staining) for >10 months. Additionally, tet*NGN3*-HIEs maintained inducible expression after storage in liquid nitrogen (data not shown).

Induction of enteroendocrine cell differentiation

To confirm that doxycycline treatment alone did not induce EEC differentiation in HIEs, we measured mRNA transcript levels after treating the parental (non-transduced) jejunum HIEs with 0 or 1 µg/mL doxycycline. We quantitated the mRNA levels of the enterochromaffin cell markers *CHGA* and *TPH1* and the enterocyte marker villin (VIL1) by quantitative polymerase chain reaction (qPCR) (**Fig. 2B**). No significant difference between treatment groups was present in any of the cell markers examined, indicating that doxycycline alone does not impact EEC differentiation in the absence of *NGN3* expression (**Fig. 2B**).

In a complementary approach to demonstrate that induction of tet*NGN3* increases EEC differentiation, we correlated the increase in *NGN3* and *CHGA* transcripts in tet*NGN3*-HIEs treated with 0, 0.1, and 1 µg/mL doxycycline, and compared gene expression in the three different HIE formats (i.e., 3D culture, flat monolayers, and transwell monolayers), summarized in **Table 3**. Overall, we observed a doxycycline dose-dependent increase in both *NGN3* and *CHGA* expression in all three formats of the tet*NGN3*-HIEs. Treatment with 1 µg/mL doxycycline significantly increased both enterochromaffin cell markers in all three culture formats (**Fig. 2C**). However, there were some notable differences in the expression profiles between each type of HIE format. Treating 3D tet*NGN3*-HIEs with 0.1 µg/mL doxycycline induced *NGN3* and *CHGA* expression to a lesser degree than 0.1 µg/mL doxycycline treatment of flat or transwell monolayers (**Fig. 2C**), which may be due to limited penetrance of doxycycline through the Matrigel used for 3D cultures. Further, transwell monolayers treated with 0.1 µg/mL doxycycline have a greater fold induction of *NGN3* and *CHGA*

expression than in flat monolayers (**Fig. 2C**). This difference may be the result of greater cell surface contact with the media in transwell monolayers, which have both apical and basolateral access to the media, than in flat monolayers. Together, these results demonstrate that the inducible tet*NGN3*-HIEs are a tunable and versatile system for increased differentiation of enterochromaffin cells in each of the HIE culture formats.

Characterization of epithelial cell types present in tetNGN3-HIEs

To assess the impact of *NGN3* overexpression on HIE morphology, we treated 3D and transwell monolayer preparations of the tet*NGN3*-HIEs with 0, 0.1, and 1 µg/mL doxycycline (**Fig. 3A, B**). Hematoxylin and eosin (H&E) staining of 3D (**Fig. 3A**) and transwell monolayers (**Fig. 3B**) showed only minor alterations in morphology upon induction with 0.1 µg/mL doxycycline, primarily larger nuclei and increased cell height (**Fig. 3B, middle panel**). Strong induction with 1 µg/mL doxycycline resulted in more significant morphological changes. In the 3D tet*NGN3*-HIEs, there was a marked increase in luminal (apical) cell debris (**Fig. 3A, right panel**), and in transwell monolayers we observed larger nuclei and a discontinuous apical membrane with increased shedding of cellular material (**Fig. 3B, right panel**). Further, we examined the ultrastructure of the tet*NGN3*-HIEs using transmission electron microscopy of 3D HIEs treated for 5 days with 0 or 1 µg/mL doxycycline in differentiation media (**Fig. 3C and 3D**). Most cells observed in the 0 µg/mL doxycycline-treated tet*NGN3*-HIEs had the basolateral nuclei, apical microvilli, and brush border characteristic of enterocytes (**Fig. 3C**). As expected, in tet*NGN3*-HIEs treated with 1 µg/mL doxycycline, we observed

more EECs based on greater numbers of cells with electron-dense granules, including cells open to the lumen of the 3D enteroid (**Fig. 3D**).

'Differentiation' of HIEs by exclusion of Wnt3a from the culture media drives maturation of the different epithelial cell types [14, 17, 21, 42, 43], so we next used RT-qPCR to determine whether *NGN3* induction altered expression of cell lineage-specific marker genes in differentiated HIEs. For this we tested markers for Paneth cells (*LYSZ*), crypt base columnar stem cells (*LGR5*), goblet cells (*MUC2)*, and enterocytes [villin (*VIL1)* and sucrase isomaltase (*SI*)] (**Table 2**). First, we observed no difference in differentiation marker expression between the parental HIE line and the uninduced tet*NGN3*-HIEs, indicating that lentivirus transduction itself did not cause alterations in HIE cell differentiation (data not shown). In 3D tet*NGN3*-HIEs (**Fig. 4A, left panel**), doxycycline induction caused no significant changes in cell lineage-specific gene expression, and while *SI* exhibited a trend for lower levels, expression of *VIL1* remained unchanged. Further, in tet*NGN3*-HIE flat monolayers the overall gene expression levels were similar to the 3D tet*NGN3*-HIEs and no significant changes in lineage-specific marker genes were observed (**Fig. 4A, right panel**).

To gain further insight into the broader impacts of *NGN3* overexpression, we performed global transcriptional analysis of mRNA (RNA-seq) isolated from tet*NGN3*-HIEs cultured in transwell format in the absence or presence of 1 µg/mL doxycycline for 5 days. Comparison of the expression levels across 31 genes indicated a dramatic increase in the abundance of *NGN3* and *CHGA* transcripts (**Fig. 4B**) However, there was relatively little change in genes involved in tight junctions, or markers of Paneth, goblet or tuft cell lineages. In contrast, all markers of enterocytes decreased modestly,

with log_2 fold changes of less than 2 (**Fig. 4B, Table 4**). Similar to the H&E staining (**Fig. 3**), immunofluorescence microscopy of 3D cultures and transwell monolayers demonstrated that the tet*NGN3*-HIEs maintained a polarized cell layer upon doxycycline treatment, as demonstrated by apical localization of phospho-ezrin, SI, and sodium-glucose transporter 1 (**Fig. 4C-E**). Finally, we examined whether *NGN3* overexpression altered goblet cell numbers in the tet*NGN3*-HIEs. Immunostaining for Muc2 in non-induced or induced (1 µg/mL doxycycline) 3D tet*NGN3*-HIEs showed that induction of *NGN3* expression did not decrease the number of Muc2-positive cells (**Fig. 4F**), which is consistent with the lack of changes in *MUC2* gene expression between 0 and 1 µg/mL doxycycline treatments found by qPCR and RNA-seq analyses (**Fig. 4A,B**). Taken together, inducible *NGN3* overexpression significantly increases the EEC population, but this does not substantially change the transcript levels of other differentiated cell types or the morphological characteristics of these enteroids.

tetNGN3-HIEs secrete serotonin in response to physiological stimuli

The enterochromaffin cell subtype is an important source of serotonin-mediated signaling, which has multiple effects on intestinal homeostasis, and disruptions in serotonin signaling have been shown to contribute to several GI disorders [44-50]. Serotonin is synthesized via the conversion of L-tryptophan by the enzyme tryptophan hydroxylase (Tph1), and stored in secretory vesicles for stimulus-driven secretion [51]. Therefore, we tested if induction of *NGN3* overexpression in HIEs increased serotonin response to biological stimuli *in vitro*. We confirmed that both *CHGA* and *TPH1* gene expression are upregulated in doxycycline-induced tet*NGN3*-HIEs (**Fig. 5A**). Further,

we showed that doxycycline induction (1 µg/mL) increased the number of ChgA and serotonin double-positive cells by fluorescence of 3D tet*NGN3*-HIEs (**Fig. 5B**). These indicate an increase in the number of serotonin-secreting enterochromaffin cells.

We next characterized the physiological response of the tet*NGN3*-HIE-derived enterochromaffin cells to stimuli previously shown to elicit serotonin secretion by other enterochromaffin model systems [52, 53]. A previous study found that mouse enterochromaffin cells secrete serotonin in response to norepinephrine and isovalerate [52]. Norepinephrine is a neurotransmitter important for communication between the gut and the enteric nervous system, particularly in response to infection or injury [54]. Isovalerate is a fatty acid metabolite likely generated by the microbiome, particularly by amino acid fermenting bacteria such as from the Clostridial, Bacillus, Lactobacillus, Streptococcus and Proteobacteria groups [55]. We quantified serotonin secretion into the media of flat monolayers of tet*NGN3*-HIEs, induced with 0 or 1 µg/mL doxycycline, and treated with different concentrations of norepinephrine or isovalerate. After stimulation with these agonists, supernatants were collected to measure serotonin secretion using a serotonin ELISA. We found that norepinephrine treatment of induced tet*NGN3*-HIEs stimulated a significant and dose-dependent increase in serotonin secretion, but no increase in serotonin secretion was observed from the non-induced tet*NGN3*-HIEs ($p<0.05$, $p<0.0001$) (**Fig. 5C**). Interestingly, treatment with up to 500 µM isovalerate did not stimulate measurable serotonin secretion in either the non-induced or the doxycycline-induced tet*NGN3*-HIEs (**Fig. 5D**).

To determine if our model is responsive to other microbial stimuli, we tested whether rotavirus (RV) infection, a common diarrhea-causing enteric virus, stimulates

serotonin secretion from tet*NGN3*-HIEs. Previous studies in both human enterochromaffin cell lines, and in mice found that RV infects both enterocytes and ChgA- and serotonin-positive enterochromaffin cells and stimulates serotonin secretion [12, 53]. Furthermore, HIEs are a new model for RV infection and enterochromaffin cells in HIEs support RV infection; however, whether RV infection stimulates serotonin secretion in HIEs has not been tested [13, 14]. Flat monolayers of tet*NGN3*-HIE induced with 0 or 1 µg/mL doxycycline were infected with trypsin-activated human RV (strain Ito, G3[P8]). Supernatants were harvested at 24 hr post-infection to measure serotonin secretion. RV infection significantly increased serotonin secretion in both the non-induced and doxycycline-induced tet*NGN3*-HIEs compared to mock-infected tet*NGN3*-HIEs ($p < 0.0001$) (**Fig. 5E**). Most notably, the serotonin response to RV infection was significantly greater from the doxycycline-induced tet*NGN3*-HIEs, demonstrating that the tet*NGN3*-HIEs amplify observed enterochromaffin cell responses (**Fig. 5E**).

The ability of RV to stimulate serotonin secretion in tet*NGN3*-HIEs was also tested in transwell monolayers that were induced with 0.1 µg/mL doxycycline in differentiation media for 5 days. In transwell monolayers, we were able to test serotonin secretion both apically and basolaterally after infection with RV at 1 hpi, 12 hpi, and 24 hpi (**Fig. 5F and 5G**). At 12 hpi, RV-infected transwell monolayers secreted significantly more serotonin into the basolateral compartment than mock-infected monolayers ($p<0.05$) (**Fig. 5G**), while apical serotonin secretion was not significantly increased (**Fig. 5F**). By 24 hpi, there was significantly more serotonin secretion both apically and basolaterally from RV-infected than mock-infected monolayers ($p<0.01$) (**Fig. 5G and 5F**). These data indicate that serotonin is primarily secreted basolaterally from the

monolayer, particularly early in RV infection, but both basolateral and apical serotonin secretion is detected later in infection. Finally we confirmed that the doxycycline-induced enterochromaffin cells are susceptible to RV infection by immunofluorescence confocal microscopy. At 12 hpi, the tet*NGN3*-HIE transwell monolayers were fix and stained for ChgA and the RV non-structural protein 2 (NSP2), which shows co-immunostaining of cells for ChgA and NSP2 (**Fig. 5H**) that is consistent with the known susceptibility of enterochromaffin cells to RV infection [12, 13, 53].

***tet*NGN3-*HIEs differentiate into multiple enteroendocrine cell types**

To identify other EEC types that are present in the induced tet*NGN3*-HIEs, we examined the RNA-seq data from doxycycline-induced te*tNGN3*-HIEs for expression of marker genes predominantly expressed in the seven EEC subtypes, as well as marker genes for enterochromaffin cells. We found that expression of each of the EEC marker genes was upregulated to varying degrees (**Fig. 6A, Table 4**), suggesting that doxycycline treatment of the tet*NGN3*-HIEs could induce the other EEC cell types in addition to enterochromaffin cells. These results are supported by positive immunostaining for GLP-1 distinct from ChgA-positive cells in tet*NGN3*-HIE monolayers when induced with 1 µg/mL doxycycline (**Fig. 6B**). To test if doxycycline-induced tet*NGN3*-HIEs functionally amplified the physiological response of these EEC subtypes, we quantified gut hormones known to be secreted by different EEC types after stimulation with norepinephrine or infection with RV, as in the experiments above (**Fig. 6C-F**). We did not detect secreted hormones from uninduced tet*NGN3*-HIE monolayers after stimulation with norepinephrine or RV infection, with the exception of monocyte

chemoattractant protein-1 (MCP-1), which is also known to be produced by enterocytes (**Fig. 6C and 6D**). In contrast, tet*NGN3*-HIE monolayers induced with 1 µg/mL doxycycline exhibited increased secretion of MCP-1 and glucose-dependent insulinotropic peptide (GIP, from K cells) in response to 5 µM norepinephrine (**Fig. 6B**). Of note, norepinephrine did not stimulate PYY (L cells) or ghrelin (P/D1 cells). Further, in response to RV infection, the induced tet*NGN3*-HIEs secreted large quantities of MCP-1 and GIP and moderate amounts of PYY and ghrelin (**Fig. 6E**), and this response was absent in uninduced tet*NGN3* HIEs (**Fig. 6D**). Norepinephrine and RV infection did not stimulate PP (pancreatic polypeptide; PP cells also known as F cells) secretion, which is primarily produced in pancreatic cells and only rarely in the intestine [56]. Together, these data show that our tet*NGN3*-HIE model drives the differentiation of multiple functional EEC subtypes that secrete gut hormones in response to biologically relevant stimuli.

Discussion

Limitations of the available human EEC systems have made it challenging to comprehensively study the molecular physiology of EECs. In this study, we engineered a HIE line to have inducible overexpression of *NGN3* that enable vast upregulation of EEC numbers in the HIE. For the characterization of the tet*NGN3*-HIEs, we initially focused on enterochromaffin cells because they are the dominant intestinal EEC subtype and of great interest for EEC biology, and serve a key role in sensing/responding to microbial metabolites and intestinal pathophysiology [57-59]. We demonstrated that doxycycline-induced *NGN3* overexpression in human jejunal intestinal enteroids increased EECs, as measured by mRNA and protein expression of the endocrine marker *CHGA*. This response was doxycycline-dose dependent, demonstrating that the tet*NGN3*-HIEs allow for “tunable” customization of the number of EECs in different HIE formats (e.g., 3D, flat monolayers, and transwell monolayers). Further, in response to known stimuli, differentiated tet*NGN3*-HIEs release serotonin and several gut hormones characteristic of K cell, L cell, and enterochromaffin cell populations in a single culture system [12, 52, 53].

The tet*NGN3*-HIE model system described in this work overcomes some of the limitations associated with the existing models of EECs. In contrast to primary EECs isolated from tissue and cancer-derived cell lines, HIOs and HIEs are more robust and renewable model systems for studying EECs [29, 52, 60, 61]. However, like the intestine, few EECs spontaneously develop in both HIOs and HIEs, so the rarity of EEC cells remains a limitation of native organoid/enteroid cultures. Thus, increasing *NGN3* expression to drive EEC differentiation, as has been done in recent work with HIOs, is

418 an effective strategy to increase the abundance of EECs for study [29, 40, 62]. In HIOs,
419 *NGN3* overexpression increased the number of ChgA-positive cells to 5% using
420 adenovirus-based constitutive expression and to 23% using lentivirus-based
421 doxycycline-inducible expression [29, 40, 62]. This is comparable to our results with the
422 tet*NGN3*-HIEs wherein we obtained 40% ChgA-positive cells using a lentivirus-based
423 inducible *NGN3* overexpression strategy. These results indicate that for both HIOs and
424 HIEs, stably engineering the stem cell to have inducible expression of *NGN3* is an
425 efficient approach to drive differentiation of higher numbers of EECs.

426 Together, the use of inducible *NGN3* expression in HIOs and HIEs establish
427 complementary systems that will be widely useful to interrogate different aspects of
428 EEC interactions in the GI tract. In the tet*NGN3*-HIEs model, the HIEs are derived from
429 undifferentiated adult stem cells, and will therefore be particularly useful for studies of
430 adult intestinal epithelial cell expression, function, and physiology. Indeed, isolation,
431 establishment, and transduction of enteroids from individual patients to assess EEC
432 function or response to drug treatments may be a future strategy for personalized
433 medicine [63]. Whereas HIOs are composed of both epithelial and mesenchymal cells,
434 HIEs consist of only epithelial cells so the tet*NGN3*-HIEs allow direct study of EEC
435 interactions with other intestinal epithelial cells. Additionally, co-culture studies that
436 combine the tet*NGN3*-HIEs with other cell types, such as immune cells, endothelial
437 cells, and neurons, will be facilitated by the adaptability of HIEs to different culture
438 formats (3D, 2D, and transwells), which is unique to HIE cultures. Finally, induction and
439 differentiation of tet*NGN3*-HIEs yields EECs in 6-7 days, which may be a simpler and

faster system for generating increased numbers of EECs for higher-throughput studies of EEC responses to microbial, diet, or environmental stimuli.

The induced EECs from tet*NGN3*-HIEs exhibit strong functional responses to both norepinephrine and RV infection. Both norepinephrine and RV infection increased secretion of serotonin, MCP-1, and GIP, but RV infection also elicited secretion of PYY and ghrelin. Thus, this system displays distinct functional responses to different stimuli. HIEs have been established as a new, biologically relevant system to study RV-induced gut hormone secretion. RV infects enterochromaffin cells in HIEs and induces serotonin secretion both in mice and *in vitro* from GOT1 cells [12-14]. Here we show that RV infection of tet*NGN3*-HIEs induced serotonin secretion, but this response was significantly amplified by doxycycline-induction to increase EECs. Using transwell monolayers, we were able to show that serotonin is secreted both apically and basolaterally, though it is possible that some basolateral-to-apical diffusion of serotonin occurs, potentially through damaged tight junctions [12, 53]. RV also induced secretion of GIP, PYY, and ghrelin, which was only detected from doxycycline-induced tet*NGN3*-HIEs and indicates that biological responses from rare EECs may be missed in native enteroids. These finding highlights the potential tet*NGN3*-HIEs have for molecular discovery, because secretion of GIP, PYY, and ghrelin during RV infection has not previously been identified, so whether RV infects these EEC subtypes or secretion of these hormones occurs through other signaling pathways merits future investigation [64]. Finally, since insults to the epithelium elevate levels of catecholamines (e.g., norepinephrine), the sensitivity of tet*NGN3*-HIEs to norepinephrine makes them a good

462 model for co-culture studies to measure EEC responses to inflammation or infection [48,
463 87].

464 The tet*NGN3*-HIEs are a robust and versatile system for induction of EECs, but
465 some limitations and unknowns about this new model remain. First, the induction of
466 EECs in this system requires lentivirus-integration of a recombinant *NGN3* gene,
467 making these an engineered intestinal organoid system. An alternative approach to
468 induce endogenous EECs in mouse intestinal organoids was established through the
469 combined inhibition of WNT, Notch, and EGFR (i.e., MAPK) signaling pathways [65].
470 This method leads to increased EEC differentiation, with a concomitant decrease in
471 Paneth and goblet cell numbers [65]. In contrast, the tet*NGN3*-HIEs maintained markers
472 of both Paneth and goblet cells, suggesting that Ngn3 expression alone is insufficient to
473 abolish these other lineage pathways. Second, using this HIE model, we observed
474 increases in most EEC subtypes by RNA-seq and measured hormone secretion from
475 enterochromaffin, L, K, and P/D1 cell subtypes. Although beyond the scope of this
476 study, further studies are needed to determine whether the other subtypes are also
477 functionally responsive to stimuli [66-71]. Finally, the tet*NGN3*-HIEs did not secrete
478 serotonin in response to the short-chain fatty acid isovalerate, in contrast to recent
479 studies using enteroids derived from ChgA-EGFP reporter mice (segment not specified)
480 [52]. Inherent differences between the two systems, such as different receptor
481 expression between human and mouse or between intestinal segments, may account
482 for the different responses.

483 The tet*NGN3*-HIE system is a new and powerful tool for investigating the roles of
484 EECs in microbial-environment-host communication, infection, inflammation,

485 metabolism. Doxycycline-induction of the tet*NGN3*-HIEs generates large numbers of
486 EECs and amplifies EEC responses to biologically relevant stimuli, yet these cultures
487 retain the salient characteristics of HIEs. Further, this is an adaptable system of in terms
488 of both regulating the number of EECs and culture formats, which enables greater
489 throughput and functional characterization of EEC responses to a multitude of stimuli.
490 The ability of tet*NGN3*-HIEs to differentially respond to norepinephrine and RV infection
491 suggests this new model system is well-suited to study the EEC modulatory effects of
492 commensal microbes, microbial metabolites, pathogens and inflammatory mediators
493 involved in epithelial health and disease.
494

Materials and Methods

Establishment of HIE cultures

Human intestinal enteroid (HIE) cultures were generated from crypts isolated from the jejunal tissues of adult patients undergoing bariatric surgery as previously described [13]. These established cultures were obtained at Baylor College of Medicine through the Texas Medical Center Digestive Diseases Center Study Design and Clinical Research Core. Three-dimensional HIE cultures were prepared from the tissue samples and maintained in culture as described previously [13, 17]. For these studies, jejunum HIEs from patient J2 were used. Complete medium without growth factors (CMGF-) and complete medium with growth factors (CMGF+) were prepared as previously described [13, 17]. Briefly, CMGF- consisted of Advanced Dulbecco's modified Eagle medium (DMEM)/F-12 medium (Invitrogen) supplemented with 100 U/mL penicillin-streptomycin (Invitrogen), 10 mM HEPES buffer (Invitrogen), and 1X GlutaMAX (Invitrogen). CMGF+ consisted of CMGF- medium with 50% (v/v) Wnt3A-conditioned medium, 20% (v/v) R-spondin conditioned medium, 10% (v/v) Noggin-conditioned medium, 1X B-27 supplement (Invitrogen), 1X N-2 supplement (Invitrogen), 1 mM N-acetylcysteine (Sigma-Aldrich), 50 ng/mL mouse epidermal growth factor (EGF) (Invitrogen), 10 mM nicotinamide (Sigma-Aldrich, St. Louis, MO), 10 nM Leu-Gastrin I (Sigma-Aldrich), 500 nM A-83-01 (Tocris Bioscience), and 10 nM SB202190 (Sigma-Aldrich).

Differentiation medium consisted of the same components as CMGF+ without Wnt3A conditioned medium, R-spondin conditioned medium, SB202190, and nicotinamide and only 5% (v/v) Noggin conditioned medium. High Wnt CMGF+ (hW-CMGF+), for creating and maintaining lentivirus-transduced HIEs, consisted of CMGF+

518 mixed with an additional 50% (v/v) Wnt3a conditioned medium. All HIEs were passaged
519 in phenol red-free, growth factor-reduced Matrigel (Corning).
520
521 *Creation of NGN3-expressing HIEs*
522 Tetracycline-inducible tet*NGN3*-expressing HIEs were created using lentivirus
523 transduction. The tet*NGN3* lentivirus transfer plasmid was in the pINDUCER backbone
524 and a kind gift from Dr. Noah Shroyer and Dr. Jim Wells [62, 72]. The tet*NGN3*
525 lentiviruses were packaged and harvested in-house with the packaging plasmid
526 psPAX2, a gift from Dr. Didier Trono (Addgene plasmid #12260), and the envelope
527 plasmid pCMV-VSV-G, a gift from Dr. Bob Weinberg (Addgene plasmid #8454), as
528 described in more detail previously [73]. Virus packaging was assessed using Lenti-X
529 GoStix (Clontech) but virus titers were not otherwise measured. Densely seeded
530 jejunum HIEs were grown in hW-CMGF+ for one week to increase stem cell counts.
531 HIEs were dissociated from Matrigel with ice-cold 1X phosphate buffered saline (PBS)
532 and pipetted into 1.7 mL centrifugation tubes for centrifugation in a swinging bucket
533 rotor at 200 x *g* for 5 min at 4°C. Supernatant was removed, HIEs were resuspended
534 and washed twice with 1 mL ice-cold 1X PBS and centrifuged using the same
535 conditions. Supernatants were removed and HIEs resuspended with lentivirus inoculum
536 consisting of 8 µg/mL polybrene (EMD Millipore), 10 µM Y-27632 Rock inhibitor (Tocris
537 Biosciences), 50 µL tet*NGN3* lentivirus, and freshly made hW-CMGF+ for a total volume
538 of 200 µL. HIEs were incubated with the inoculum in closed centrifugation tubes for 24
539 hr at 37°C in a humidified 5% CO_2 incubator. After 24 hr, HIEs were centrifuged again
540 and washed twice with ice-cold 1X PBS followed by suspension in Matrigel drops on a

24-well plate. Following Matrigel polymerization in the incubator for 10 min, 500 µL of hW-CMGF+ medium was added to the well. Media was changed every other day for one week before passaging and selecting with 200 µg/mL Geneticin (VWR). We refer to this transduced line as tet*NGN3*-HIEs, and they were grown in hW-CMGF+ with 200 µg/mL Geneticin.

Preparation and differentiation of HIE monolayers

HIE monolayers were prepared from three-dimensional cultures and seeded into flat 96-well plates or transwells as described previously [21, 42]. In brief, 96-wells or transwell inserts (Costar, cat. no. 3413) were pre-treated with Matrigel diluted in 1XPBS (1:40) and incubated at 37°C. 3D HIEs were lifted from Matrigel and washed with an ice cold solution of 0.5 mM EDTA in 1X PBS and dissociated with 0.05% trypsin/0.5 mM EDTA for 4 min at 37°C. Trypsin was inactivated with CMGF- + 10% FBS and the cell solution was pipetted vigorously and filtered using a 40 µm nylon cell strainer (Falcon, cat. no. 352340) to dissociate into single cells. Then cells were centrifuged for 5 min at 400 x *g*, resuspended with CMGF+ and 10 µM Y-27632 Rock inhibitor, and plated into prepared wells. After 48 hr in CMGF+ and 10 µM Y-27632 Rock inhibitor, the medium was changed to differentiation media with the addition of 10 µM Y-27632 Rock inhibitor and indicated concentrations of doxycycline (Fisher Scientific). Differentiation medium with Y-27632 and doxycycline was changed every day for 4-5 days to differentiate cells.

Immunofluorescence of HIE monolayers

Two-dimensional HIE flat monolayers were fixed using the BD Cytofix/Cytoperm kit (BD Biosciences, cat. no. 554714) according to manufacturer instructions. Primary antibodies were diluted in BD Perm/Wash buffer and (**Table 1**) were incubated at 4°C overnight. Primary antibodies were recognized by the appropriate secondary antibodies (**Table 1**) and incubated for 1 hr at room temperature. Nuclei were stained with DAPI (Thermo Fisher Scientific, cat. no. R37606) for 5 min at room temperature and washed with 1X PBS for imaging and storage.

Immunofluorescence of paraffin-embedded sections

Three-dimensional (3D) HIEs embedded in Matrigel were gently removed and transferred to 1 mL syringes. The cells were then fixed in 4% (v/v) paraformaldehyde solution for 1 hr at room temperature. After fixation, cells were deposited into a cassette for paraffin embedding. For transwell cross-sections HIE membranes were cut from transwells, fixed in 4% (v/v) paraformaldehyde solution for 1 hr at room temperature and placed into cassettes for paraffin embedding. Paraffin-embedded sections of 7 µm in thickness were subjected to a series of dehydration steps. Epitope retrieval was performed by incubating slides with Vector Labs Antigen Unmasking Solution Citrate Buffer pH 6 (Vector labs, cat no. H-3300) for 20 min at 100°C in a steamer. Slides were then blocked for 1 hr at room temperature in 10% goat and/or donkey serum. Primary antibodies (**Table 1**) were incubated at 4°C overnight. Primary antibodies were recognized by the appropriate secondary antibodies (**Table 1**) and incubated for 1 hr at room temperature. Nuclei were stained with DAPI (Thermo Fisher Scientific, cat. no.

R37606) for 5 min at room temperature. All slides were cover-slipped with mounting media (Life Technologies) and imaged.

Transmission Electron Microscopy

Three-dimensional HIEs embedded in Matrigel were primary fixed in a solution of 2% paraformaldehyde + 2.5% glutaraldehyde + 2 mM calcium chloride in 0.1 M cacodylate buffer (pH = 7.4) for 5-7 days at 4°C. They were post-fixed in 1% osmium tetroxide in 0.1 M cacodylate buffer for 1 hr and en bloc stained with saturated aqueous uranyl acetate. After a routine dehydration sequence, tissue pieces were gradually infiltrated in a gradient series of Spurr's Low Viscosity resin and ethanol, then embedded in fresh Spurr's resin and polymerized at 60° C for 3 days. 55-60 nm thin sections were cut on a Leica UC7 ultra-microtome using a Diatome Ultra 45 diamond knife. Sections were viewed on a Hitachi H7500 transmission electron microscope set to 80kV. Images were collected using an AMT XR-16 digital camera and AMT Image Capture, v602.600.51 software.

Microscopy and image analysis

tet*NGN3*-HIEs were imaged with widefield epifluorescence on a Nikon TiE inverted microscope and an upright Nikon Eclipse 90i microscope using a SPECTRA X LED light source (Lumencor) as well as a Nikon A1plus point scanning confocal microscope for fluorescence imaging. The following objectives were used: 10X Plan Fluor (NA 0.3) phase contrast objective, 20X Plan Apo (NA 0.75) differential interference contrast (DIC) objective, a 40X Apo DIC water objective, and a Plan Apo

608 VC 60X Oil DIC objective. Fluorescence images were recorded using either an ORCA-
609 Flash 4.0 sCMOS camera (Hamamatsu) or a CoolSNAP HQ2 camera (Photometrics),
610 and color images for H&E sections were recorded using a DS-Fi1-U2 camera (Nikon).
611 Nikon Elements Advanced Research v4.5 software was used for data acquisition and
612 image analysis.

613 To quantify ChgA-positive cells in 3D and monolayer tet*NGN3*-HIEs, images
614 were analyzed using Nikon Elements software. Individual images were processed with a
615 4 µm size threshold by channel to reduce noise from nonspecific staining. Images were
616 morphologically separated using a 3x3 matrix, and objects touching the borders were
617 removed. The percent of positive cells was the number of Alexa Fluor 488-positive
618 objects divided by the number of DAPI-stained detected nuclei. At least 5 images per
619 condition were analyzed with an average of 140 (3D cultures) or 1400 (flat monolayers)
620 nuclei per image.

621

622 *RNA extraction, reverse transcription, and real-time PCR*

623 tet*NGN3*-HIEs were rinsed once with ice cold 1XPBS and transferred to a
624 centrifugation tube (technical duplicates were combined into a single tube). Cells were
625 lysed by the addition of 1 mL of TRIZOL Reagent (Invitrogen) and mixed thoroughly
626 using a vortex mixer for 30 seconds. Chloroform (200 µL) was added, the samples were
627 mixed again, and then incubated for 5 min at room temperature. The phases were
628 separated by centrifugation at 14,000 x *g* for 10 min, and the aqueous phase was
629 moved to a new tube (~400 µL). Total RNA was then isolated using the RNeasy
630 Isolation Kit (Qiagen) according to the manufacturer's instructions. RNA was eluted in

20 µL sterile nuclease free water (Fischer Scientific). RNA concentration and purity were determined by absorbance at 260 nm and 280 nm using a spectrophotometer (DS-11, DeNovix). RNA (200 ng) was treated with DNase (Ambion Turbo DNA-free) to remove any contaminating genomic DNA per manufacturer's directions, and then cDNA was synthesized from purified total RNA using SuperScript III reverse transcriptase (Invitrogen) according to the manufacturer's instructions. Reaction components included random hexamers (Integrated DNA Technologies), 10 mM dNTPs (New England Biosciences), and approximately 2 ng of RNA. No reverse transcriptase controls were included by omitting SuperScript III.

Real time PCR reactions were performed in triplicate with the following reaction components: 1 µL cDNA, 0.25 µL of 20 mM forward and reverse primer (**Table 2**), 10 µL Power SYBR Green PCR MasterMix (Applied Biosystems), and 8.5 µL nuclease free water (Fisher Scientific). Real-time PCR was performed using QuantStudio real time thermocycler (Applied Biosciences) under the following conditions: 95°C 10 min, 40 cycles of 95°C for 15 seconds, followed by 60°C for 1 min, when data was recorded. A melting curve between 60°C and 95°C was performed. No template controls were included by substituting water for the cDNA in the reaction. C_T values of technical replicates were averaged for each independent biological experiment and normalized to the expression of the 18S ribosomal subunit. Data graphed are representative of 3 experiments (n=3 biological replicates, with 3 technical replicates in each experiment).

Preparation of HIE transwells for RNA-sequencing and transcriptional analysis

To assess the transcriptional profile changes of tet*NGN3-HIEs* during doxycycline induction. HIE monolayers were prepared on transwells and differentiated as described above. The total RNA was extracted from transwells in the presence or absence of 1 µg/ml doxycycline using the same protocol as for RT and qPCR described above. rRNA integrity was checked on an Agilent 2100 bioanalyzer from six independent biological replicates per condition. Paired-end Illumina sequencing was performed on mRNA enriched samples by Novogene (USA) following the standard work-flow procedure. Raw sequence reads were mapped to human genome hg19 using STAR software to generate the number of fragments per kilobase per million mapped reads (FPKM) for each gene. Ratios of transcript abundance per group were based on the $\log_2$ FPKM value in 1 µg/ml doxycycline condition relative to the 0 µg/mL doxycycline condition were used to determine the fold change in gene expression. Samples were filtered for those containing >10% N value, presence of adaptor sequences, and quality. Greater than 97% of reads in each sample were clean reads post-filtering with error rates ≤ 0.03%. Pearson correlation coefficients between samples were between 0.92 and 0.97 R^2 values. In total, 10,741 genes were differentially expressed between the groups (5,870 up-regulated, 4,871 down-regulated) as indicated by DESeq2 analysis using a padj value <0.05, and a $\log_2$ fold change >1, q-value <0.005.

Isovalerate and norepinephrine stimulation

After four days in differentiation medium and induced with 0, 0.1, or 1 µg/mL doxycycline, confluent HIE monolayers were washed with 1XPBS. Isovalerate (Sigma-

Aldrich) and noradrenaline bitartrate (Tocris Bioscience) solutions were prepared in 1X PBS and added to the HIE monolayers. Monolayers were incubated for 2 hr at 37°C and 5% CO_2. Following incubation, supernatants were harvested and kept at -20°C for downstream analysis. PrestoBlue Cell Viability Reagent (ThermoFisher Scientific), a resazurin-based assay, was utilized according to manufacturer's recommended protocols. Fluorescence intensity of reduced resazurin (560-610 nm, Infinite F200Pro, Tecan) measures metabolic activity of the cells and was used as an indication of cell viability.

Rotavirus infection of HIE monolayers

African green monkey kidney (MA104) cells were cultured in DMEM supplemented with 10% (v/v) fetal bovine serum (Corning). Ito RV (G3[P8]) was propagated in MA104 cells in serum-free DMEM in the presence of 1 µg/mL Worthington's Trypsin (Worthington Biochemical). After harvest, stocks were subjected to three freeze/thaw cycles. Plaque assays with MA104 cells were used to determine the titers of the viral preparations. The tet*NGN3*-HIE flat or transwell monolayers were induced with 0, 0.1, or 1 µg/mL doxycycline in differentiation media for 4-5 days. For infection, the confluent HIE monolayers were washed once with CMGF-. Mock MA104 cell lysates and Ito RV were treated with 10 µg/mL Worthington's trypsin for 30 min at 37°C. Then the tet*NGN3*-HIE monolayers were treated with an inoculum of CMGF- with MA104 cell lysate or Ito RV. Cells were infected basolaterally following observations that this method results in more efficient infections (Blutt, Crawford, and Estes, unpublished data). Transwell and flat monolayers were incubated for 1 hr or 2 hr,

699 respectively, at 37°C with 5% CO_2. Following incubation, the supernatants were
700 removed and replaced with differentiation media and returned to the incubator. For the 1
701 hpi timepoint, supernatants were collected 5 min after washing inoculum. Supernatants
702 were harvested and kept at -20°C for downstream analyses.
703
704 *Measurement of serotonin release*
705 Serotonin secretion by HIEs following stimulation with norepinephrine,
706 isovalerate, or RV infection was quantified by ELISA (Eagle Biosciences) according to
707 the manufacturer's instructions. A standard curve of known serotonin concentrations
708 was plotted against optical density at 450 nm with a limit of detection of 2.6 ng/mL
709 (Infinite F200Pro, Tecan).
710
711 *Measurement of metabolic hormones*
712 Hormone secretion was quantified by Luminex assay (Human Metabolic
713 Hormone Magnetic Bead Panel, HMHEMAG-34K, EMD Millipore) according to
714 manufacturer's standard protocol. Supernatants following stimulation with
715 norepinephrine or RV infection were assayed for the amount of secreted amylin (active),
716 C-Peptide, ghrelin (active), GIP (total), GLP-1 (total), glucagon, IL-6, leptin, MCP-1, PP,
717 PYY (total), and TNF-α. Limits of detection of the assay are: amylin 11.81 pg/ml, C-
718 Peptide 13.28 pg/ml, ghrelin 9.40 pg/ml, GIP 0.33 pg/ml, GLP-1 1.11 pg/ml, glucagon
719 12.73 pg/ml, IL-6 3.75 pg/ml, leptin 54.16 pg/ml, MCP-1 8.57 pg/ml, PP 0.68 pg/ml, PYY
720 11.18 pg/ml, and TNF-α <0.14 pg/ml.
721

Statistical analysis

Biostatistical analyses were performed using GraphPad Prism (version 7) software (GraphPad Inc., La Jolla, CA). Comparisons were made with either One-way or Two-way Analysis of Variance (ANOVA) and Tukey's post hoc multiple comparisons test when appropriate. Differences between the groups were considered significant at $p < 0.05$ (*), and the data are presented as mean ± standard deviation. All authors had access to the study data, reviewed, and approved the final manuscript.

Acknowledgments

We would like to thank Dr. Noah Shroyer for providing the tet*NGN3* plasmid. The BCM Medical Scientist Training Program and the Integrative Molecular and Biomedical Sciences Graduate Program provided additional trainee support (A.C.G). We would like to thank Xi-Lei (Shelly) Zeng and Xiaomin Yu of the Digestive Diseases Center Enteroid Core for their help with maintaining the enteroid culturing and enteroid media. We thank Debra Townley and Michael A. Mancini, Ph.D. of the Integrated Microscopy Core for their help with transmission electron microscopy of the enteroids.

References

[1] Ferraris RP, Lee PP, Diamond JM. Origin of regional and species differences in intestinal glucose uptake. Am J Physiol 1989;257(5 Pt 1):G689-97.

[2] Bergman EN. Energy contributions of volatile fatty acids from the gastrointestinal tract in various species. Physiol Rev 1990;70(2):567-90.

[3] Worthington JJ, Reimann F, Gribble FM. Enteroendocrine cells-sensory sentinels of the intestinal environment and orchestrators of mucosal immunity. Mucosal Immunol 2018;11(1):3-20.

[4] Schonhoff SE, Giel-Moloney M, Leiter AB. Minireview: Development and differentiation of gut endocrine cells. Endocrinology 2004;145(6):2639-44.

[5] Ahlman H, Nilsson. The gut as the largest endocrine organ in the body. Ann Oncol 2001;12 Suppl 2:S63-8.

[6] Sternini C, Anselmi L, Rozengurt E. Enteroendocrine cells: a site of 'taste' in gastrointestinal chemosensing. Curr Opin Endocrinol Diabetes Obes 2008;15(1):73-8.

[7] Rehfeld JF. The new biology of gastrointestinal hormones. Physiol Rev 1998;78(4):1087-108.

[8] Sjolund K, Sanden G, Hakanson R, Sundler F. Endocrine cells in human intestine: an immunocytochemical study. Gastroenterology 1983;85(5):1120-30.

[9] Solcia E, Capella C, Buffa R, Usellini L, Fiocca R, Frigerio B, Tenti P, Sessa F. The diffuse endocrine-paracrine system of the gut in health and disease: ultrastructural features. Scand J Gastroenterol Suppl 1981;70:25-36.

[10] Roth KA, Gordon JI. Spatial differentiation of the intestinal epithelium: analysis of enteroendocrine cells containing immunoreactive serotonin, secretin, and substance P in normal and transgenic mice. Proc Natl Acad Sci U S A 1990;87(16):6408-12.

[11] Andrews PL, Davis CJ, Bingham S, Davidson HI, Hawthorn J, Maskell L. The abdominal visceral innervation and the emetic reflex: pathways, pharmacology, and plasticity. Can J Physiol Pharmacol 1990;68(2):325-45.

[12] Hagbom M, Istrate C, Engblom D, Karlsson T, Rodriguez-Diaz J, Buesa J, Taylor JA, Loitto VM, Magnusson KE, Ahlman H, Lundgren O, Svensson L. Rotavirus stimulates release of serotonin (5-HT) from human enterochromaffin cells and activates brain structures involved in nausea and vomiting. PLoS Pathog 2011;7(7):e1002115.

[13] Saxena K, Blutt SE, Ettayebi K, Zeng XL, Broughman JR, Crawford SE, Karandikar UC, Sastri NP, Conner ME, Opekun AR, Graham DY, Qureshi W, Sherman V, Foulke-Abel J, In J, Kovbasnjuk O, Zachos NC, Donowitz M, Estes MK. Human Intestinal Enteroids: a New Model To Study Human Rotavirus Infection, Host Restriction, and Pathophysiology. J Virol 2016;90(1):43-56.

[14] Zachos NC, Kovbasnjuk O, Foulke-Abel J, In J, Blutt SE, de Jonge HR, Estes MK, Donowitz M. Human Enteroids/Colonoids and Intestinal Organoids Functionally Recapitulate Normal Intestinal Physiology and Pathophysiology. J Biol Chem 2016;291(8):3759-66.

[15] Clevers H. Modeling Development and Disease with Organoids. Cell 2016;165(7):1586-97.

[16] Bartfeld S. Modeling infectious diseases and host-microbe interactions in gastrointestinal organoids. Dev Biol 2016;420(2):262-70.

[17] Sato T, Stange DE, Ferrante M, Vries RG, Van Es JH, Van den Brink S, Van Houdt WJ, Pronk A, Van Gorp J, Siersema PD, Clevers H. Long-term expansion of epithelial organoids from human colon, adenoma, adenocarcinoma, and Barrett's epithelium. Gastroenterology 2011;141(5):1762-72.

[18] Sato T, Vries RG, Snippert HJ, van de Wetering M, Barker N, Stange DE, van Es JH, Abo A, Kujala P, Peters PJ, Clevers H. Single Lgr5 stem cells build crypt-villus structures in vitro without a mesenchymal niche. Nature 2009;459(7244):262-5.

[19] Foulke-Abel J, In J, Kovbasnjuk O, Zachos NC, Ettayebi K, Blutt SE, Hyser JM, Zeng XL, Crawford SE, Broughman JR, Estes MK, Donowitz M. Human enteroids as an ex-vivo model of host-pathogen interactions in the gastrointestinal tract. Exp Biol Med (Maywood) 2014;239(9):1124-34.

[20] Foulke-Abel J, In J, Yin J, Zachos NC, Kovbasnjuk O, Estes MK, de Jonge H, Donowitz M. Human Enteroids as a Model of Upper Small Intestinal Ion Transport Physiology and Pathophysiology. Gastroenterology 2016;150(3):638-49 e8.

[21] Ettayebi K, Crawford SE, Murakami K, Broughman JR, Karandikar U, Tenge VR, Neill FH, Blutt SE, Zeng XL, Qu L, Kou B, Opekun AR, Burrin D, Graham DY, Ramani S, Atmar RL, Estes MK. Replication of human noroviruses in stem cell-derived human enteroids. Science 2016;353(6306):1387-93.

[22] Apelqvist A, Li H, Sommer L, Beatus P, Anderson DJ, Honjo T, Hrabe de Angelis M, Lendahl U, Edlund H. Notch signalling controls pancreatic cell differentiation. Nature 1999;400(6747):877-81.

[23] Gradwohl G, Dierich A, LeMeur M, Guillemot F. neurogenin3 is required for the development of the four endocrine cell lineages of the pancreas. Proc Natl Acad Sci U S A 2000;97(4):1607-11.

[24] Jenny M, Uhl C, Roche C, Duluc I, Guillermin V, Guillemot F, Jensen J, Kedinger M, Gradwohl G. Neurogenin3 is differentially required for endocrine cell fate specification in the intestinal and gastric epithelium. EMBO J 2002;21(23):6338-47.

[25] Jensen J, Heller RS, Funder-Nielsen T, Pedersen EE, Lindsell C, Weinmaster G, Madsen OD, Serup P. Independent development of pancreatic alpha- and beta-cells from neurogenin3-expressing precursors: a role for the notch pathway in repression of premature differentiation. Diabetes 2000;49(2):163-76.

[26] Schwitzgebel VM, Scheel DW, Conners JR, Kalamaras J, Lee JE, Anderson DJ, Sussel L, Johnson JD, German MS. Expression of neurogenin3 reveals an islet cell precursor population in the pancreas. Development 2000;127(16):3533-42.

[27] Suissa Y, Magenheim J, Stolovich-Rain M, Hija A, Collombat P, Mansouri A, Sussel L, Sosa-Pineda B, McCracken K, Wells JM, Heller RS, Dor Y, Glaser B. Gastrin: a distinct fate of neurogenin3 positive progenitor cells in the embryonic pancreas. PLoS One 2013;8(8):e70397.

[28] McGrath PS, Watson CL, Ingram C, Helmrath MA, Wells JM. The Basic Helix-Loop-Helix Transcription Factor NEUROG3 Is Required for Development of the Human Endocrine Pancreas. Diabetes 2015;64(7):2497-505.

[29] Spence JR, Mayhew CN, Rankin SA, Kuhar MF, Vallance JE, Tolle K, Hoskins EE, Kalinichenko VV, Wells SI, Zorn AM, Shroyer NF, Wells JM. Directed differentiation of human pluripotent stem cells into intestinal tissue in vitro. Nature 2011;470(7332):105-9.

[30] Sinagoga KL, Wells JM. Generating human intestinal tissues from pluripotent stem cells to study development and disease. EMBO J 2015;34(9):1149-63.

[31] Pinney SE, Oliver-Krasinski J, Ernst L, Hughes N, Patel P, Stoffers DA, Russo P, De Leon DD. Neonatal diabetes and congenital malabsorptive diarrhea attributable to a novel mutation in the human neurogenin-3 gene coding sequence. J Clin Endocrinol Metab 2011;96(7):1960-5.

[32] Rubio-Cabezas O, Jensen JN, Hodgson MI, Codner E, Ellard S, Serup P, Hattersley AT. Permanent Neonatal Diabetes and Enteric Anendocrinosis Associated With Biallelic Mutations in NEUROG3. Diabetes 2011;60(4):1349-53.

[33] German-Diaz M, Rodriguez-Gil Y, Cruz-Rojo J, Charbit-Henrion F, Cerf-Bensussan N, Manzanares-Lopez Manzanares J, Moreno-Villares JM. A New Case of Congenital Malabsorptive Diarrhea and Diabetes Secondary to Mutant Neurogenin-3. Pediatrics 2017;140(2):e1-6.

[34] Jensen JN, Rosenberg LC, Hecksher-Sorensen J, Serup P. Mutant neurogenin-3 in congenital malabsorptive diarrhea. N Engl J Med 2007;356(17):1781-2.

[35] Unlusoy Aksu A, Egritas Gurkan O, Sari S, Demirtas Z, Turkyilmaz C, Poyraz A, Dalgic B. Mutant neurogenin-3 in a Turkish boy with congenital malabsorptive diarrhea. Pediatr Int 2016;58(5):379-82.

[36] Wang J, Cortina G, Wu SV, Tran R, Cho JH, Tsai MJ, Bailey TJ, Jamrich M, Ament ME, Treem WR, Hill ID, Vargas JH, Gershman G, Farmer DG, Reyen L, Martin MG. Mutant neurogenin-3 in congenital malabsorptive diarrhea. N Engl J Med 2006;355(3):270-80.

[37] Ueo T, Imayoshi I, Kobayashi T, Ohtsuka T, Seno H, Nakase H, Chiba T, Kageyama R. The role of Hes genes in intestinal development, homeostasis and tumor formation. Development 2012;139(6):1071-82.

[38] Chen YJ, Finkbeiner SR, Weinblatt D, Emmett MJ, Tameire F, Yousefi M, Yang C, Maehr R, Zhou Q, Shemer R, Dor Y, Li C, Spence JR, Stanger BZ. De novo formation of insulin-producing "neo-beta cell islets" from intestinal crypts. Cell Rep 2014;6(6):1046-58.

[39] Ootani A, Li X, Sangiorgi E, Ho QT, Ueno H, Toda S, Sugihara H, Fujimoto K, Weissman IL, Capecchi MR, Kuo CJ. Sustained in vitro intestinal epithelial culture within a Wnt-dependent stem cell niche. Nat Med 2009;15(6):701-6.

[40] Sinagoga KL, McCauley HA, Munera JO, Reynolds NA, Enriquez JR, Watson C, Yang HC, Helmrath MA, Wells JM. Deriving functional human enteroendocrine cells from pluripotent stem cells. Development 2018;145(19).

[41] Wade PR, Westfall JA. Ultrastructure of enterochromaffin cells and associated neural and vascular elements in the mouse duodenum. Cell Tissue Res 1985;241(3):557-63.

[42] VanDussen KL, Marinshaw JM, Shaikh N, Miyoshi H, Moon C, Tarr PI, Ciorba MA, Stappenbeck TS. Development of an enhanced human gastrointestinal epithelial culture system to facilitate patient-based assays. Gut 2015;64(6):911-20.

[43] Leushacke M, Barker N, Pin C. Quantifying Lgr5-positive stem cell behaviour in the pyloric epithelium. Sci Rep 2016;6:21923.
[44] Bertrand PP, Barajas-Espinosa A, Neshat S, Bertrand RL, Lomax AE. Analysis of real-time serotonin (5-HT) availability during experimental colitis in mouse. Am J Physiol Gastrointest Liver Physiol 2010;298(3):G446-55.
[45] Linden DR, Foley KF, McQuoid C, Simpson J, Sharkey KA, Mawe GM. Serotonin transporter function and expression are reduced in mice with TNBS-induced colitis. Neurogastroenterol Motil 2005;17(4):565-74.
[46] Wheatcroft J, Wakelin D, Smith A, Mahoney CR, Mawe G, Spiller R. Enterochromaffin cell hyperplasia and decreased serotonin transporter in a mouse model of postinfectious bowel dysfunction. Neurogastroenterol Motil 2005;17(6):863-70.
[47] Bischoff SC, Mailer R, Pabst O, Weier G, Sedlik W, Li Z, Chen JJ, Murphy DL, Gershon MD. Role of serotonin in intestinal inflammation: knockout of serotonin reuptake transporter exacerbates 2,4,6-trinitrobenzene sulfonic acid colitis in mice. Am J Physiol Gastrointest Liver Physiol 2009;296(3):G685-95.
[48] Coates MD, Mahoney CR, Linden DR, Sampson JE, Chen J, Blaszyk H, Crowell MD, Sharkey KA, Gershon MD, Mawe GM, Moses PL. Molecular defects in mucosal serotonin content and decreased serotonin reuptake transporter in ulcerative colitis and irritable bowel syndrome. Gastroenterology 2004;126(7):1657-64.
[49] Khan WI. The Role of 5-HT Dysregulation in Inflammatory Bowel Disease. Gastroenterol Hepatol (N Y) 2013;9(4):259-61.
[50] Wang Y, Gong H, Lopez R, Lian L, Kiran RP, Soffer EE, Shen B. Correlation between serum serotonin and endoscopy inflammation scores in patients with ileal pouches. J Crohns Colitis 2013;7(4):e133-42.
[51] Thomson AB, Drozdowski L, Iordache C, Thomson BK, Vermeire S, Clandinin MT, Wild G. Small bowel review: Normal physiology, part 2. Dig Dis Sci 2003;48(8):1565-81.
[52] Bellono NW, Bayrer JR, Leitch DB, Castro J, Zhang C, O'Donnell TA, Brierley SM, Ingraham HA, Julius D. Enterochromaffin Cells Are Gut Chemosensors that Couple to Sensory Neural Pathways. Cell 2017;170(1):185-98 e16.
[53] Bialowas S, Hagbom M, Nordgren J, Karlsson T, Sharma S, Magnusson KE, Svensson L. Rotavirus and Serotonin Cross-Talk in Diarrhoea. PLoS One 2016;11(7):e0159660.
[54] Gabanyi I, Muller PA, Feighery L, Oliveira TY, Costa-Pinto FA, Mucida D. Neuro-immune Interactions Drive Tissue Programming in Intestinal Macrophages. Cell 2016;164(3):378-91.
[55] Neis EP, Dejong CH, Rensen SS. The role of microbial amino acid metabolism in host metabolism. Nutrients 2015;7(4):2930-46.
[56] Cox HM. Neuropeptide Y receptors; antisecretory control of intestinal epithelial function. Auton Neurosci 2007;133(1):76-85.
[57] O'Mahony SM, Clarke G, Borre YE, Dinan TG, Cryan JF. Serotonin, tryptophan metabolism and the brain-gut-microbiome axis. Behav Brain Res 2015;277:32-48.

[58] Yano JM, Yu K, Donaldson GP, Shastri GG, Ann P, Ma L, Nagler CR, Ismagilov RF, Mazmanian SK, Hsiao EY. Indigenous bacteria from the gut microbiota regulate host serotonin biosynthesis. Cell 2015;161(2):264-76.

[59] Evrensel A, Ceylan ME. The Gut-Brain Axis: The Missing Link in Depression. Clin Psychopharmacol Neurosci 2015;13(3):239-44.

[60] Tsuruta T, Saito S, Osaki Y, Hamada A, Aoki-Yoshida A, Sonoyama K. Organoids as an ex vivo model for studying the serotonin system in the murine small intestine and colon epithelium. Biochem Biophys Res Commun 2016;474(1):161-7.

[61] Kishida K, Pearce SC, Yu S, Gao N, Ferraris RP. Nutrient sensing by absorptive and secretory progenies of small intestinal stem cells. Am J Physiol Gastrointest Liver Physiol 2017;312(6):G592-G605.

[62] McCracken KW, Cata EM, Crawford CM, Sinagoga KL, Schumacher M, Rockich BE, Tsai YH, Mayhew CN, Spence JR, Zavros Y, Wells JM. Modelling human development and disease in pluripotent stem-cell-derived gastric organoids. Nature 2014;516(7531):400-4.

[63] Dekkers JF, Berkers G, Kruisselbrink E, Vonk A, de Jonge HR, Janssens HM, Bronsveld I, van de Graaf EA, Nieuwenhuis EE, Houwen RH, Vleggaar FP, Escher JC, de Rijke YB, Majoor CJ, Heijerman HG, de Winter-de Groot KM, Clevers H, van der Ent CK, Beekman JM. Characterizing responses to CFTR-modulating drugs using rectal organoids derived from subjects with cystic fibrosis. Science translational medicine 2016;8(344):344ra84.

[64] Rollo EE, Kumar KP, Reich NC, Cohen J, Angel J, Greenberg HB, Sheth R, Anderson J, Oh B, Hempson SJ, Mackow ER, Shaw RD. The epithelial cell response to rotavirus infection. J Immunol 1999;163(8):4442-52.

[65] Basak O, Beumer J, Wiebrands K, Seno H, van Oudenaarden A, Clevers H. Induced Quiescence of Lgr5+ Stem Cells in Intestinal Organoids Enables Differentiation of Hormone-Producing Enteroendocrine Cells. Cell Stem Cell 2017;20(2):177-90 e4.

[66] Grun D, Lyubimova A, Kester L, Wiebrands K, Basak O, Sasaki N, Clevers H, van Oudenaarden A. Single-cell messenger RNA sequencing reveals rare intestinal cell types. Nature 2015;525(7568):251-5.

[67] Petersen N, Reimann F, Bartfeld S, Farin HF, Ringnalda FC, Vries RG, van den Brink S, Clevers H, Gribble FM, de Koning EJ. Generation of L cells in mouse and human small intestine organoids. Diabetes 2014;63(2):410-20.

[68] Zietek T, Rath E, Haller D, Daniel H. Intestinal organoids for assessing nutrient transport, sensing and incretin secretion. Sci Rep 2015;5:16831.

[69] Petersen N, Reimann F, van Es JH, van den Berg BM, Kroone C, Pais R, Jansen E, Clevers H, Gribble FM, de Koning EJ. Targeting development of incretin-producing cells increases insulin secretion. J Clin Invest 2015;125(1):379-85.

[70] Bohorquez DV, Samsa LA, Roholt A, Medicetty S, Chandra R, Liddle RA. An enteroendocrine cell-enteric glia connection revealed by 3D electron microscopy. PLoS One 2014;9(2):e89881.

[71] Pattison AM, Blomain ES, Merlino DJ, Wang F, Crissey MA, Kraft CL, Rappaport JA, Snook AE, Lynch JP, Waldman SA. Intestinal Enteroids Model Guanylate

Cyclase C-Dependent Secretion Induced by Heat-Stable Enterotoxins. Infect Immun 2016;84(10):3083-91.

[72] McCracken KW, Aihara E, Martin B, Crawford CM, Broda T, Treguier J, Zhang X, Shannon JM, Montrose MH, Wells JM. Wnt/beta-catenin promotes gastric fundus specification in mice and humans. Nature 2017;541(7636):182-7.

[73] Perry JL, Ramachandran NK, Utama B, Hyser JM. Use of genetically-encoded calcium indicators for live cell calcium imaging and localization in virus-infected cells. Methods 2015;90:28-38.

[74] Criglar JM, Hu L, Crawford SE, Hyser JM, Broughman JR, Prasad BV, Estes MK. A novel form of rotavirus NSP2 and phosphorylation-dependent NSP2-NSP5 interactions are associated with viroplasm assembly. J Virol 2014;88(2):786-98.

[75] Castro I, Aguilera S, Brockhausen I, Alliende C, Quest AF, Molina C, Urzua U, Mandel U, Bahamondes V, Barrera MJ, Sanchez M, Gonzalez S, Hermoso M, Leyton C, Gonzalez MJ. Decreased salivary sulphotransferase activity correlated with inflammation and autoimmunity parameters in Sjogren's syndrome patients. Rheumatology (Oxford) 2012;51(3):482-90.

[76] Andreu P, Peignon G, Slomianny C, Taketo MM, Colnot S, Robine S, Lamarque D, Laurent-Puig P, Perret C, Romagnolo B. A genetic study of the role of the Wnt/beta-catenin signalling in Paneth cell differentiation. Dev Biol 2008;324(2):288-96.

[77] Papetti M, Augenlicht LH. MYBL2, a link between proliferation and differentiation in maturing colon epithelial cells. J Cell Physiol 2011;226(3):785-91.

[78] Gaudier E, Jarry A, Blottiere HM, de Coppet P, Buisine MP, Aubert JP, Laboisse C, Cherbut C, Hoebler C. Butyrate specifically modulates MUC gene expression in intestinal epithelial goblet cells deprived of glucose. Am J Physiol Gastrointest Liver Physiol 2004;287(6):G1168-74.

[79] Adnan H, Quach H, MacIntosh K, Antenos M, Kirby GM. Low levels of GSTA1 expression are required for Caco-2 cell proliferation. PLoS One 2012;7(12):e51739.

[80] Radek KA, Lopez-Garcia B, Hupe M, Niesman IR, Elias PM, Taupenot L, Mahata SK, O'Connor DT, Gallo RL. The neuroendocrine peptide catestatin is a cutaneous antimicrobial and induced in the skin after injury. J Invest Dermatol 2008;128(6):1525-34.

[81] Croitoru-Lamoury J, Lamoury FM, Caristo M, Suzuki K, Walker D, Takikawa O, Taylor R, Brew BJ. Interferon-gamma regulates the proliferation and differentiation of mesenchymal stem cells via activation of indoleamine 2,3 dioxygenase (IDO). PLoS One 2011;6(2):e14698.

Tables

Table 1: Antibodies used in this work

Antibody Type	Target	Species	Company	Cat#	Dilution
Primary	Muc2	Mouse	Santa Cruz	sc-515032	1:200
Primary	Sucrase Isomaltase	Mouse	Santa Cruz	sc-393470	1:100
Primary	Sodium-glucose transporter 1/ SLC5A1	Rabbit	Novus Biologicals	NBP-238748	1:100
Primary	Chromogranin A	Rabbit	Novus Biologicals	NBP-253140	1:500
Primary	Serotonin	Goat	Immunostar	20079	1:500
Primary	Phospho-Ezrin	Rabbit	Cell Signaling	3726S	1:200
Primary	Rotavirus NSP2	Guinea Pig	[74]		1:500
Secondary	Anti-goat Alexa Fluor 488	Donkey	Life Technologies	A11055	1:1,000
Secondary	Anti-rabbit Alexa Fluor 488	Donkey	Life Technologies	R37116	1:2,000
Secondary	Anti-rabbit Alexa Fluor 555	Donkey	Life Technologies	A31572	1:1,000
Secondary	Anti-guinea pig Alexa Fluor 568	Goat	Life Technologies	A11075	1:1,000
Secondary	Anti-mouse Alexa Fluor 568	Goat	Life Technologies	A11004	1:2,000

Table 2: Primers used in this work

Gene	Forward (5') Sequence	Reverse (3') Sequence	Marker of	Reference
18S	GATATGCTCATGTGGTGTTG	AATCTTCTTCAGTCGCTCCA	Housekeeping	[75]
LYZ	AAAACCCCAGGAGCAGTTAAT	CAACCCTCTTTGCACAAGCT	Paneth Cell	[76]
LGR5	CTCCCAGGTCTGGTGTGTTG	GAGGTCTAGGTAGGAGGTGAAG	Stem Cell	[77]
MUC2	CTGCACCAAGACCGTCCTCATG	GCAAGGACTGAACAAAGACTCAGA	Goblet Cell	[78]
VIL1	AGCCAGATCACTGCTGAGGT	TGGACAGGTGTTCCTCCTTC	Enterocyte	[79]
CHGA	TGTAGTGCTGAACCCCCACC	CTCTCGCCTTTCCGGATCT	Enteroendocrine	[80]
NGN3	*AGTTGGCACTGAGCAAGC*	AGTGCCGAGTTGAGGTTG	Enteroendocrine	[67]
TPH1	TGGCTGAACCTAGTTTTGCCC	CCAAAGACTCTTAGCTGTCCATC	Enteroendocrine Serotonin synthesis	[81]

Table 3: Fold Changes in *NGN3* and *CHGA* Expression with Doxycycline Treatment

tetNGN3-HIE format	***NGN3***		***CHGA***	
	0.1 µg/mL dox	1 µg/mL dox	0.1 µg/mL dox	1 µg/mL dox
3D cultures	1.5	143	14	239
Flat monolayers	12	141	54	316
Transwell monolayers	300	436	326	445

1016 **Table 4**: RNA-seq Analysis of Fold Changes in Gene Expression with Doxycycline
1017 Treatment

Gene Symbol	Gene Name	Marker of	Fold change FPKM	SD	Log_2 fold change FPKM	SD
LGR5	Leucine-rich repeat containing G protein coupled receptor 5	Stem cells	0.94	0.50	-0.28	0.842
WNT3a	Wnt family member 3A	Stem cells	0.81	0.39	-0.53	0.993
SOX9	SRY-Box 9	Stem cells	0.68	0.12	-0.58	0.267
CDH1	Cadherin 1	Tight Junctions	0.93	0.08	-0.10	0.122
CDH2	Cadherin 2	Tight Junctions	4.80	4.09	1.12	2.303
CDH3	Cadherin 3	Tight Junctions	1.12	0.23	0.14	0.285
CLDN1	Claudin1	Tight Junctions	1.43	0.29	0.49	0.302
CLDN2	Claudin 2	Tight Junctions	1.14	0.47	0.09	0.552
TJP1	Tight junction protein 1	Tight Junctions	1.03	0.08	0.03	0.114
TJP2	Tight junction protein 2	Tight Junctions	0.79	0.08	-0.35	0.143
TJP3	Tight junction protein 3	Tight Junctions	0.55	0.07	-0.88	0.159
NHE3	Solute carrier family 9 member A3	Enterocytes	0.61	0.19	-0.78	0.443
ALPI	Alkaline phosphatase	Enterocytes	0.27	0.13	-2.09	0.818
SI	Sucrose isomaltase	Enterocytes	0.29	0.25	-2.46	1.697
SGLT	Solute carrier family 5 member 1	Enterocytes	0.27	0.14	-2.07	0.837
VIL1	Villin	Enterocytes	0.57	0.04	-0.82	0.106
KRT20	Keratin 20	Enterocytes	0.41	0.17	-1.39	0.635
FABP2	Fatty acid binding protein 2	Enterocytes	0.25	0.14	-2.18	0.882
MUC2	Mucin 2	Goblet cells	1.13	0.35	0.12	0.445
TFF3	Trefoil factor 3	Goblet cells	1.04	0.17	0.04	0.239
KLF4	Kruppel-like factor 4	Goblet cells	0.57	0.09	-0.83	0.238
AGR2	Anterior gradient 2	Goblet cells	1.74	0.24	0.79	0.196
SPDEF	SAM pointed domain containing ETS transcription factor	Goblet cells	4.66	1.38	2.16	0.462
LYZ	Lysozyme	Paneth cells	0.94	0.12	-0.10	0.178
MMP7	Matrix metallopeptidase 7	Paneth cells	1.53	1.46	-0.08	1.676
DCLK1	Double cortin like kinase 1	Tuft cells	1.52	0.82	0.45	0.687
HPGD	15-hydroxyprostaglandin dehydrogenase	Tuft cells	0.33	0.21	-1.88	0.981
TRPM5	Transient receptor potential cation channel subfamily M member 5	Tuft cells	1.01	0.40	-0.08	0.593
POU2F3	POU class 2 homeobox 3	Tuft cells	0.40	0.19	-1.45	0.675
NGN3	Neurogenin-3	Enteroendocrine	428.67	141.38	8.68	0.494
CHGA	Chromogranin A	Enteroendocrine	17779.46	23032.47	13.29	1.63
TPH1	Tryptophan hydroxylase 1	Enteroendocrine	3054.77	251.17	11.17	1.25
PAX6	Paired Box 6	Enteroendocrine	75.60	43.61	5.97	0.96
NEUROD1	Neuronal differentiation 1	Enteroendocrine	5073.90	2738.32	11.83	1.39
GIP	Gastric inhibitory polypeptide	Enteroendocrine – subtype K	6926.92	3346.00	11.26	2.63

GHRL	Ghrelin prepropeptide	Enteroendocrine – subtype K	1576.15	1351.91	10.33	0.90
SST	Somatostatin	Enteroendocrine – subtype D	6733.26	3495.26	10.93	2.62
PAX4	Paired Box 4	Enteroendocrine – subtype D	3468.87	1504.07	11.32	1.22
GLP1	Glucagon-like peptide 1	Enteroendocrine – subtype L	15.62	11.63	3.54	1.13
PYY	Peptide YY	Enteroendocrine – subtype L	5.65	2.68	1.73	0.646
GAST	Gastrin	Enteroendocrine – subtype G	46.49	35.50	4.53	2.04
SCT	Secretin	Enteroendocrine – subtype S	7.37	3.617	2.301	1.47
CCK	Cholecystokinin	Enteroendocrine – subtype I	39.66	26.75	4.57	1.88
MLN	Motilin	Enteroendocrine – subtype M	146280.01	22926.82	13.55	4.13

1018

1019 **Figures**

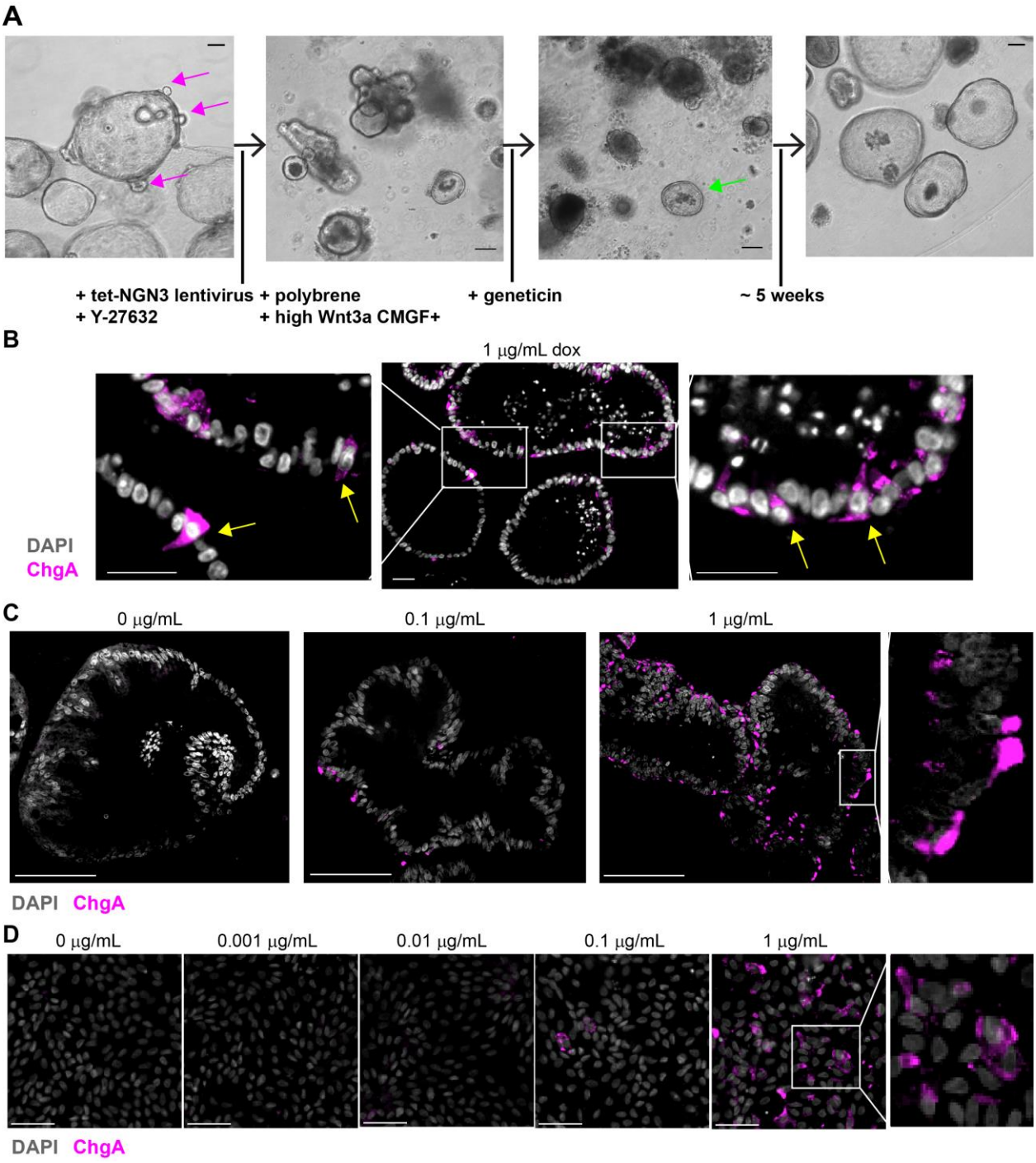

1020
1021
1022 **Figure 1: (A)** Production pipeline for creating tet*NGN3*-HIEs using lentivirus
1023 transduction. Jejunum HIEs grown in high Wnt CMGF+ media increases stem cells,
1024 evidenced by cysts and crypt buds (pink arrows), followed by inoculation with lentivirus.
1025 Reseeding the HIEs in Matrigel is followed by geneticin selection for approximately 5
1026 weeks, so that only HIEs with tet*NGN3* construct survive (green arrow) (scale bar =

100µm). Images were acquired using a 10X Plan Fluor (NA 0.3) phase contrast objective on an inverted Nikon TiE microscope with an ORCA-Flash 4.0 sCMOS camera and Nikon Elements software. **(B, C, D)** Doxycycline induces enterochromaffin marker chromogranin A (ChgA) expression in tet*NGN3*-HIEs. Tet*NGN3*-HIEs were fixed and stained for ChgA (Alexa Fluor 488 [pink]) to mark enterochromaffin cells and counterstained with DAPI (gray). **(B)** 3D tet*NGN3*-HIEs were differentiated for 4 days with 1 µg/mL doxycycline (scale bars = 25 µm). ChgA-positive cells (inset) were observed (yellow arrows). **(C, D)** tet*NGN3*-HIEs as **(C)** 3D cultures and **(D)** flat monolayers were differentiated for 4 days with 0, 0.1, and 1 µg/mL doxycycline and also 0.01 and 0.001 µg/mL doxycycline in flat monolayers. 3D culture images were acquired using a 20X Plan Apo (NA 0.75) DIC objective on an upright Nikon Eclipse 90i microscope with a Photometrics CoolSNAP HQ2 camera and Nikon Elements software (scale bar = 100 µm). Flat monolayer images were acquired using a 20X Plan Apo (NA 0.75) DIC objective on an inverted Nikon TiE microscope with an ORCA-Flash 4.0 sCMOS camera and Nikon Elements software (scale bar = 50 µm).

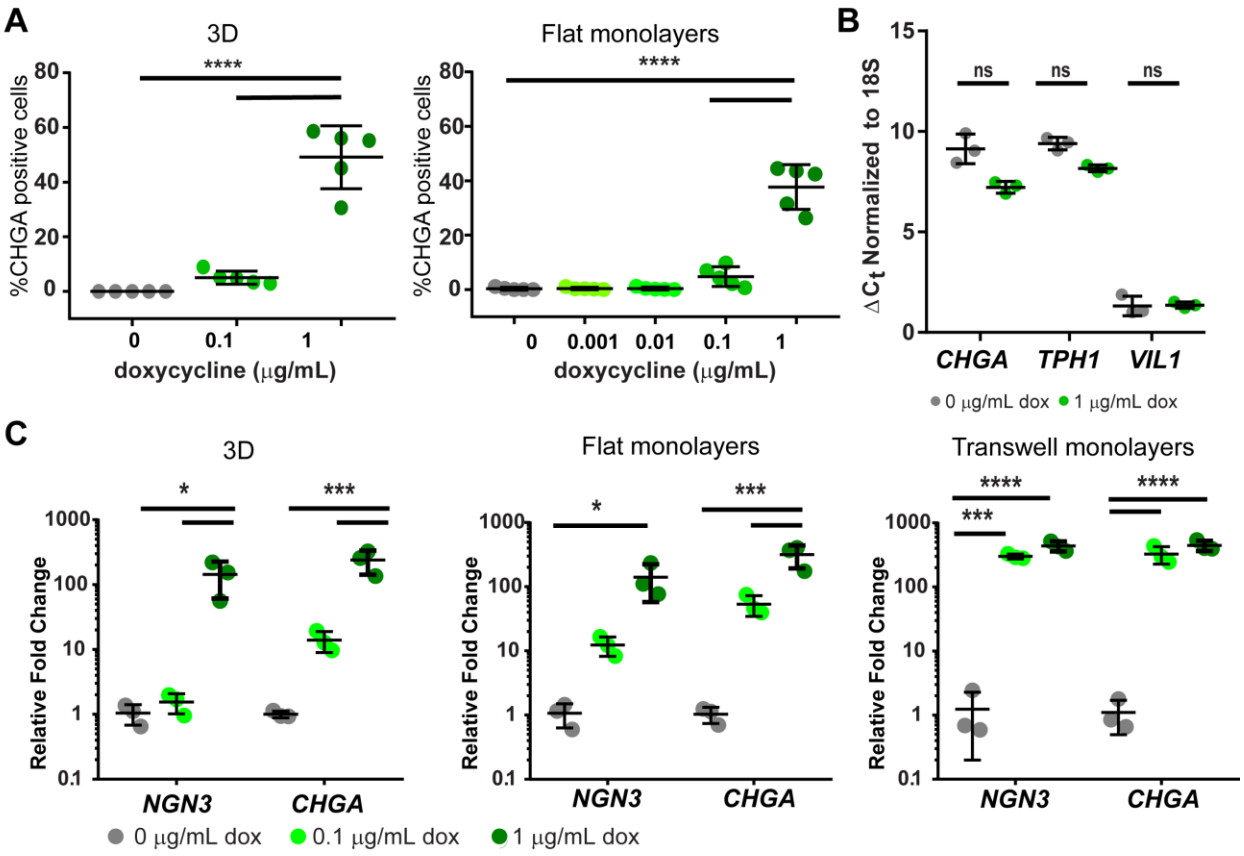

Figure 2: Doxycycline induces enteroendocrine cell lineage in tet*NGN3*-HIEs. **(A)** Increased doxycycline concentration increases the percentage of ChgA-positive cells in differentiated tet*NGN3*-HIE 3D cultures and flat monolayers. Images were analyzed with Nikon elements software with 5 images per condition with an average of 220 nuclei per image in 3D cultures and 1400 nuclei per image in flat monolayers. (n = 2 biological replicates) **(B)** qPCR of *CHGA (*chromogranin A), *TPH1* (tryptophan hydrolase-1), and *VIL1* (villin) mRNA transcripts of parental jejunum 3D enteroids were treated with 0 or 1 μg/mL doxycycline and normalized to 18S mRNA. (n = 3 biological replicates) **(C)** qPCR of *NGN3* and *CHGA* mRNA transcripts normalized to 18S mRNA transcripts in tet*NGN3* 3D cultures, flat monolayers, and transwell monolayers. (n = 3 biological replicates) (ns, not significant, *p<0.05, ***p<0.001, ****p<0.0001).

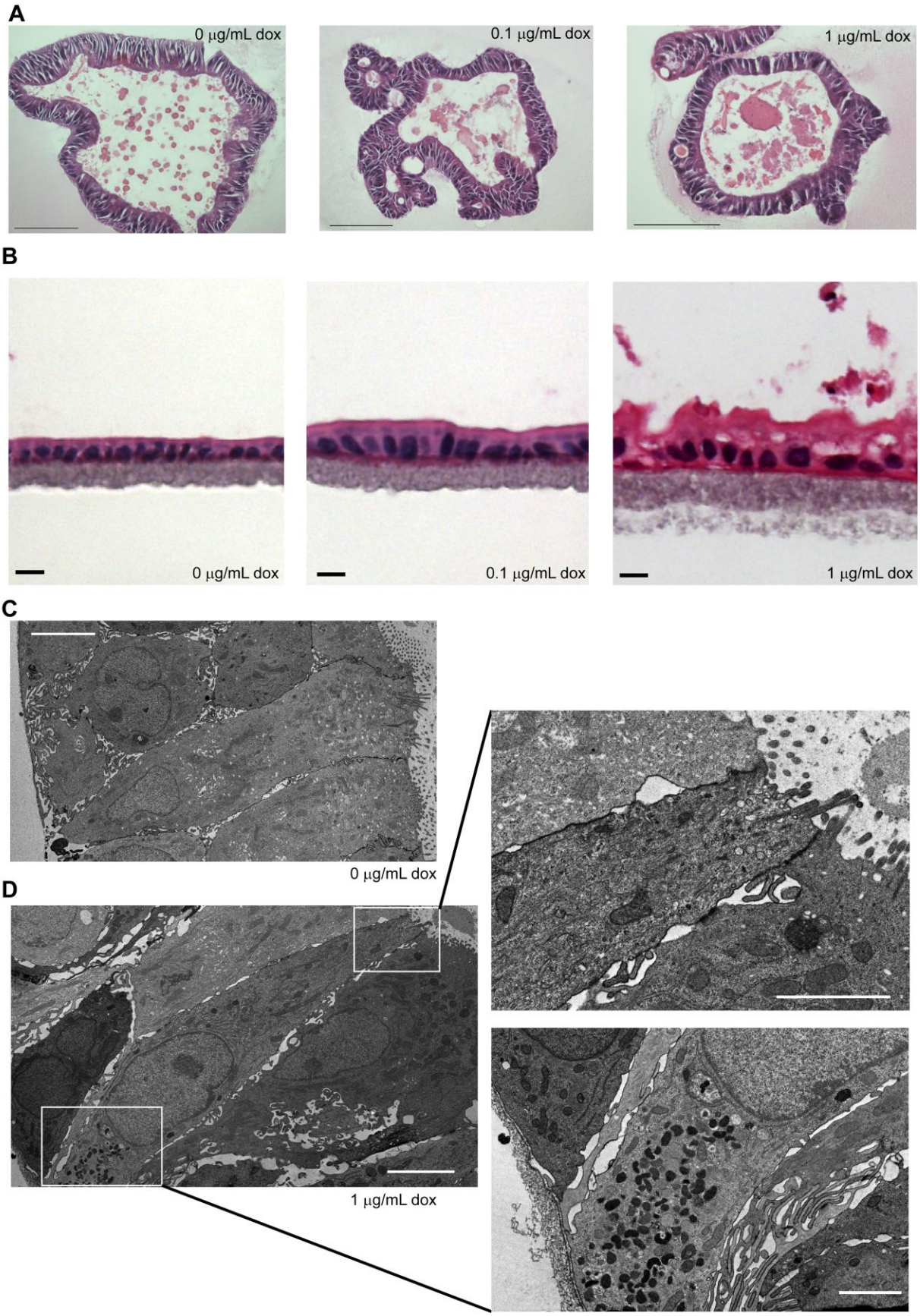

1058

Figure 3: tet*NGN3*-HIEs maintain cellular morphology in culture. Hematoxylin and eosin (H&E) stained **(A)** three-dimensional (scale bar = 100μm) and **(B)** transwell monolayer (scale bar = 10μm) tet*NGN3*-HIEs treated with 0, 0.1, or 1 μg/mL doxycycline. Images were acquired using a 20X Plan Apo (NA 0.75) DIC objective on an upright Nikon Eclipse 90i microscope with a DS-Fi1-U2 camera and Nikon Elements software. Transmission electron micrographs (TEM) H&E of three-dimensional tet*NGN3*-HIEs with **(C)** 0 μg/mL (scale bar = 4μm, 1500x magnification) or **(D)** 1 μg/mL doxycycline (left scale bars = 4μm, 1500x magnification, right scale bars = 2μm, 3000x magnification). TEM sections were viewed on a Hitachi H7500 transmission electron microscope set to 80kV and collected using an AMT XR-16 digital camera and AMT Image Capture, v602.600.51software.

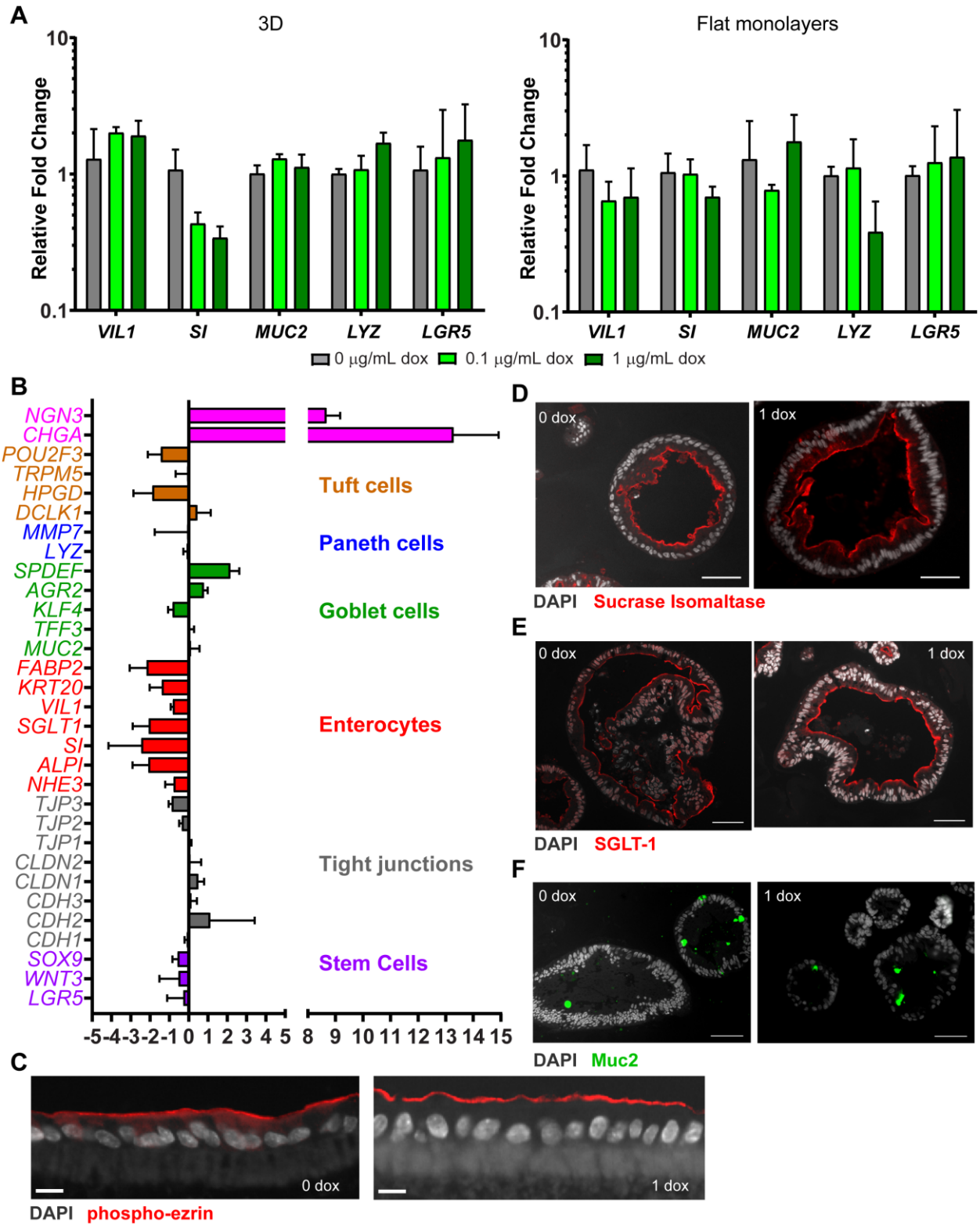

Figure 4: Characterization of epithelial cell types in doxycycline-induced tet*NGN3*-HIEs. **(A)** qPCR of cell marker mRNA transcripts normalized to 18S mRNA transcripts in

tet*NGN3*-HIE 3D cultures and flat monolayers (n = 3 biological replicates) **(B)** Log_2 fold expression of FPKM (fragments per kilobase of transcript per million mapped reads) values from RNA-seq analysis. Transwell monolayers **(C)** and 3D cultures **(D-F)** were treated with 0 or 1 µg/mL doxycycline and fixed and stained. IF staining for phospho-ezrin (Alexa Fluor 555 [red]) **(C)**, sucrase isomaltase (Alexa Fluor 555 [red]) **(D)**, and sodium-glucose transporter 1 (Alexa Fluor 555 [red]) **(E)** to mark the apical border and **(F)** for muc2 (Alexa Fluor 488 [green]) to mark goblet cells and counterstained with DAPI (blue). Images were acquired using a 20X Plan Apo (NA 0.75) DIC objective on an upright Nikon Eclipse 90i microscope with a Photometrics CoolSNAP HQ2 camera and Nikon Elements software. (**C** scale bar = 10µm, **D-F** scale bar = 50µm)

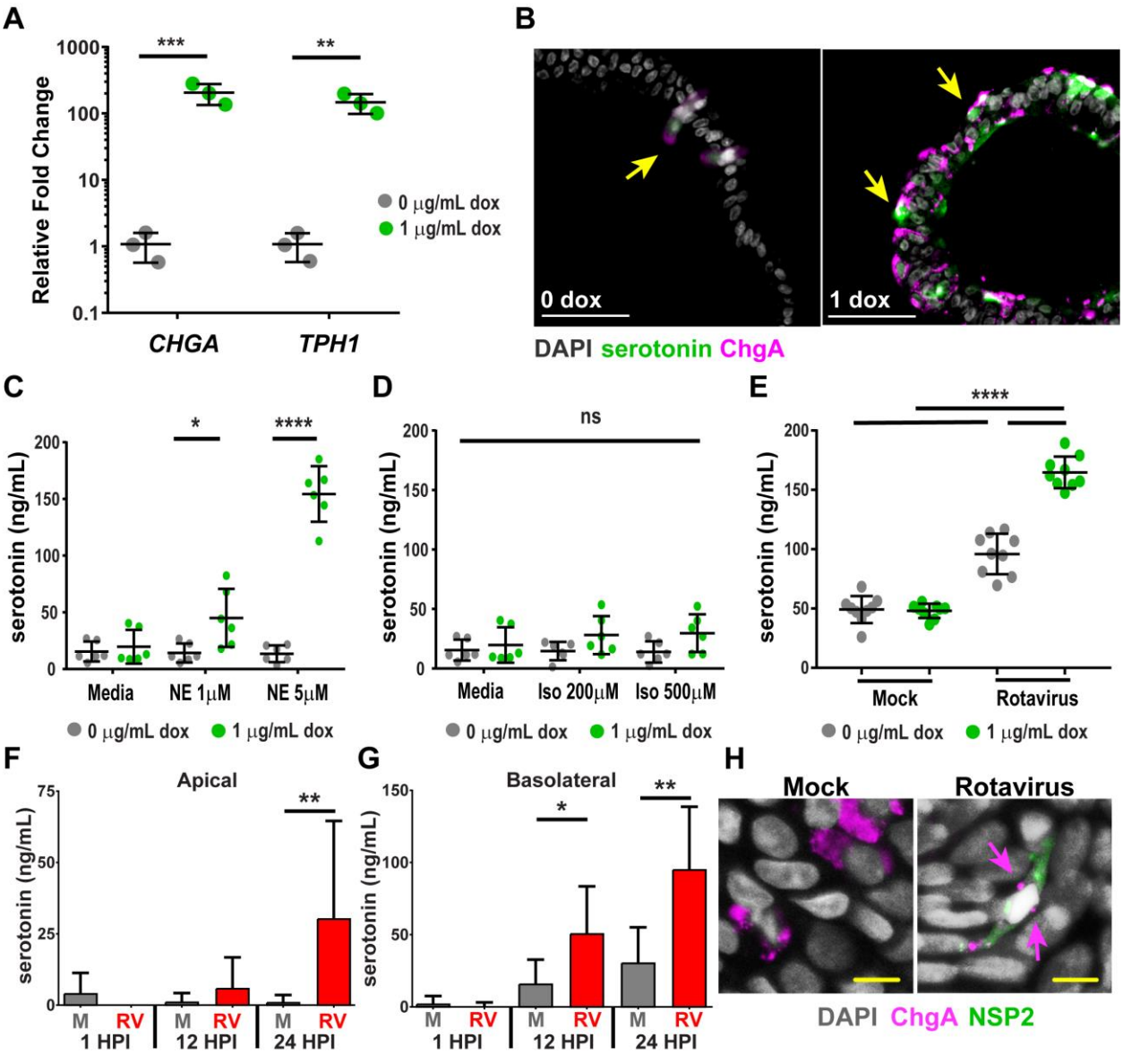

Figure 5: tet*NGN3*-HIEs produce serotonin in response to physiological stimuli. **(A)** qPCR of chromogranin A (*CHGA*) and tryptophan hydroxylase-1 (*TPH1*) mRNA transcripts normalized to 18S mRNA transcripts. (n = 3 biological replicates) **(B)** 3D tetNGN3-HIEs were treated with 0 or 1 μg/mL doxycycline (dox) and fixed and immunostained for chromogranin A (ChgA, Alexa Fluor 555 [pink]) and serotonin (Alexa Fluor 488 [green]) and counterstained with DAPI (gray). Some cells are double-positive for ChgA and seorotnin (yellow arrows). Images were acquired using a 20X Plan Apo (NA 0.75) DIC objective on an upright Nikon Eclipse 90i microscope with a Photometrics CoolSNAP HQ2 camera and Nikon Elements software (scale bar = 50 μm) **(C-E)** tet*NGN3*-HIE flat monolayers were induced with 0 or 1 μg/mL do). Serotonin release as measured by ELISA: **(C)** after 2 hr treatment with norepinephrine (NE) (n = 2 biological replicates), **(D)** after 2 hr treatment with isovalerate (Iso) (n = 2 biological replicates), and **(E)** after 24 hpi with rotavirus (n = 3 biological replicates) **(F-G)** tet*NGN3*-HIE

transwell monolayers were differentiated for 5 days with 0.1 µg/mL doxycycline and mock or rotavirus (RV)-infected. Serotonin release measured by ELISA from apical **(F)** or basal **(G)** transwell compartments. **(H)** Max intensity projection images of confocal Z-stack of transwell monolayers fixed and stained for rotavirus nonstructural protein 2 (NSP2) (Alexa Fluor 488 [green]) and ChgA (Alexa Fluor 568 [pink], arrows) and counterstained with DAPI (gray) using a Plan Apo VC 60x Oil DIC objective on a Nikon A1plus point scanning confocal microscope. (scale bar = 10µm; *p<0.05, **p<0.01,***p<0.001, ****p<0.0001).

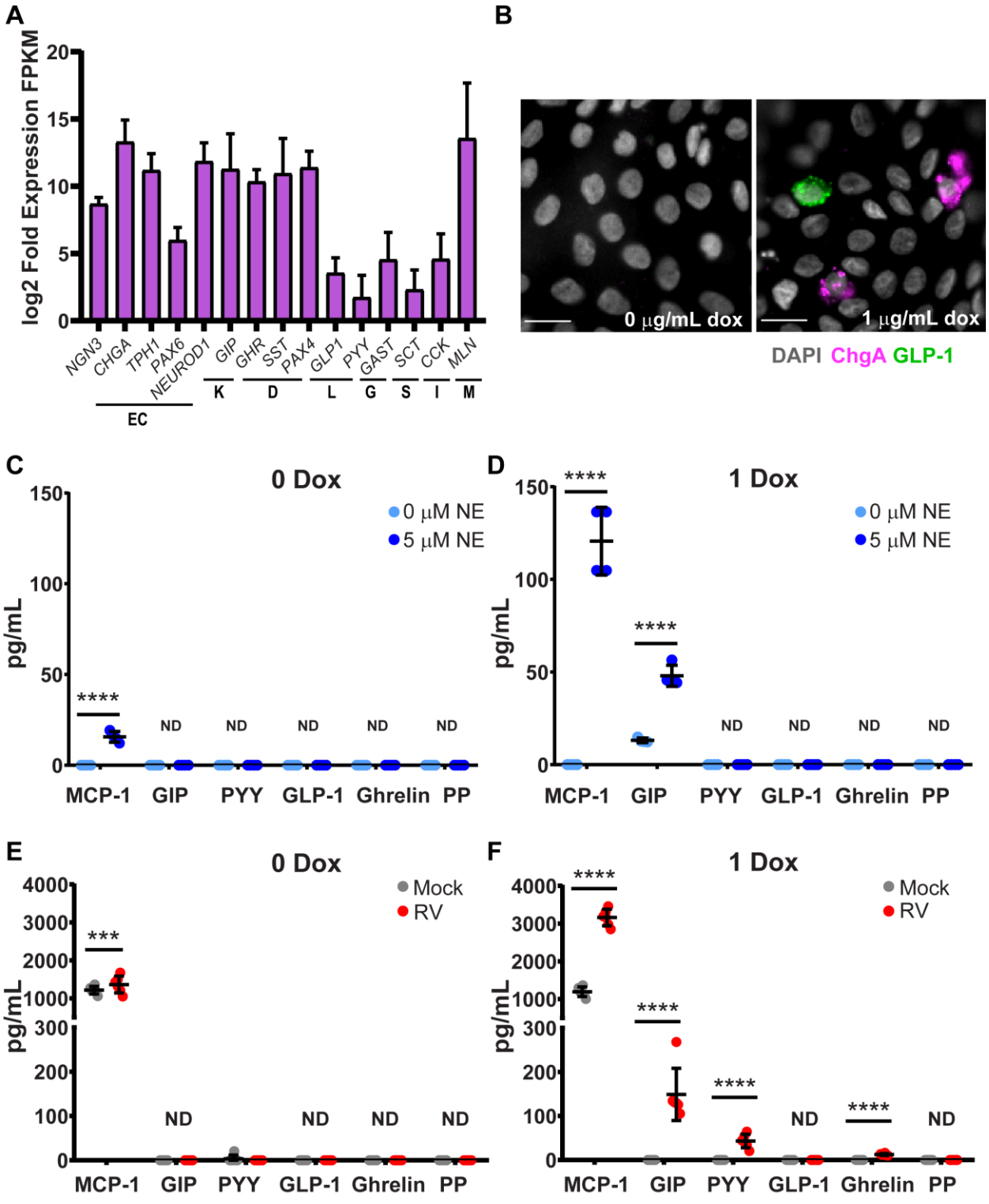

Figure 6: tet*NGN3*-HIEs differentiate into other EEC types. **(A)** Log_2 fold expression of FPKM (fragments per kilobase of transcript per million mapped reads) values from RNA-seq. **(B)** Images of monolayers fixed and stained for chromogranin A (ChgA)

(Alexa Fluor 488 [pink]) and glucagon-like peptide-1 (GLP-1) (Alexa Fluor 568 [green]) counterstained with DAPI (gray). Images were acquired using a 40X Apo (NA 1.15) DIC water objective on an inverted Nikon TiE microscope with an ORCA-Flash 4.0 sCMOS camera and Nikon Elements software. Supernatants from tet*NGN3*-HIEs were induced with 0 µg/mL doxycycline (dox) **(C,E)** or 1 µg/mL dox **(D,F)** and collected after **(C,D)** 2 hr stimulation with norepinephrine (NE) (n = 2 biological replicates) or **(E,F)** 24 hpi with rotavirus (RV) (n = 3 biological replicates) and secreted products quantitated by Luminex [monocyte chemoattractant protein-1 (MCP-1), glucose-dependent insulinotropic peptide (GIP), peptide YY (PYY), glucagon-like peptide-1 (GLP-1), pancreatic polypeptide (PP)]. (scale bar = 20µm, ***p<0.001, ****p<0.0001)

Graphical Abstract